ANTI-DIFFUSIVE AND RANDOM-SAMPLING LAGRANGIAN-REMAP SCHEMES FOR THE MULTI-CLASS LIGHTHILL-WHITHAM-RICHARDS TRAFFIC MODEL

RAIMUND BÜRGER*, CHRISTOPHE CHALONS†, AND LUIS M. VILLADA*

Abstract. The multi-class Lighthill-Whitham-Richards (MCLWR) traffic model, which distinguishes N classes of drivers differing in preferential velocity, gives rise to a system of N strongly coupled, nonlinear first-order conservation laws for the car densities as a function of distance and time. The corresponding velocities involve a hindrance function that depends on the local total density of cars. Since the eigenvalues and eigenvectors of the flux Jacobian have no closed algebraic form, characteristic-wise numerical schemes for the MCLWR model become involved. Alternative simple schemes for this model directly utilize that the velocity functions are non-negative and strictly decreasing, which allows one to construct a new class of schemes by splitting the system of conservation laws into two different first-order quasilinear systems, which are solved successively for each time iteration, namely the "Lagrangian" and "remap" steps. The new schemes are addressed as "Lagrangian-remap" (LR) schemes. One version of LR schemes incorporates recent anti-diffusive techniques for transport equations. The corresponding subclass of LR schemes are named "Lagrangian-anti-diffusive-remap" (L-AR) schemes. Alternatively, the remap step can be handled by Glimm-like random sampling, which gives rise to a statistically conservative "Lagrangian-random sampling" (L-RS) scheme that is less diffusive than other remap techniques. The LR schemes for the MCLWR model are supported by a partial analysis of the L-AR schemes for $N = 1$, which are total variation diminishing (TVD) under a suitable CFL condition and therefore converge to a weak solution, and by numerical examples for both L-AR and L-RS subclasses of schemes.

1. Introduction.

1.1. Scope. The multi-class Lighthill-Whitham-Richards (MCLWR) traffic model, proposed by Benzoni-Gavage and Colombo [2] and Wong and Wong [34], is an extension of the well-known Lighthill-Whitham-Richards kinematic traffic model [26, 30] for drivers having the same behaviour to N classes of drivers, where different classes of drivers are assumed to have different preferential velocities. The MCLWR model leads to a system of strongly coupled nonlinear first-order conservation laws

$$\partial_t \boldsymbol{\rho} + \partial_x \boldsymbol{f}(\boldsymbol{\rho}) = \mathbf{0}, \quad x \in \mathbb{R}, \quad t > 0, \tag{1.1}$$

where x is horizontal distance and either $I = \mathbb{R}$ for an unbounded highway or $I = (0, L)$ for a traffic circle of length $L > 0$, t is time, $\rho_i = \rho_i(x, t)$ is the local density of cars of class i, $\boldsymbol{\rho} = (\rho_1, \ldots, \rho_N)^{\mathrm{T}}$, $\boldsymbol{f}(\boldsymbol{\rho}) = (f_1(\boldsymbol{\rho}), \ldots, f_N(\boldsymbol{\rho}))^{\mathrm{T}}$, where

$$f_i(\boldsymbol{\rho}) = \rho_i v_i(\rho), \quad i = 1, \ldots, N, \tag{1.2}$$

and $v_i(\rho)$ is the velocity of cars of class i, which is assumed to be a function of the total density $\rho := \rho_1 + \cdots + \rho_N$. We assume that for all i, $0 \le \rho_i \le \rho \le \rho_{\max}$, where $\rho_{\max}$ is a maximum density corresponding to a bumper-to-bumper situation, and that

$$v_i(\rho) = v_i^{\max} V(\rho), \quad i = 1, \ldots, N, \tag{1.3}$$

where $v_i^{\max}$ is the preferential velocity of class i corresponding to a free highway and $V(\rho)$ is a hindrance factor that takes into account drivers' attitude to reduce speed

*CI^{2}MA and Departamento de Ingeniería Matemática, Facultad de Ciencias Físicas y Matemáticas, Universidad de Concepción, Casilla 160-C, Concepción, Chile. E-Mail: rburger@ing-mat.udec.cl, lmvillada@ing-mat.udec.cl

†Université Paris Diderot-Paris 7 & Laboratoire J.-L. Lions, U.M.R. 7598 UMPC, Boîte courrier 187, 75252 Paris Cedex 05, France. E-Mail: christophe_chalons@ljll.univ-paris-diderot.fr

in presence of other cars. The function V is usually assumed to satisfy

$$V(0) = 1, \quad V'(\rho) \leq 0 \quad \text{for } 0 \leq \rho \leq \rho_{\max}, \quad V(\rho_{\max}) = 0. \tag{1.4}$$

The numerical solution of (1.1), (1.2) is a challenge since the eigenvalues and eigenvectors of the Jacobian matrix $\mathcal{J}_{\boldsymbol{f}}(\boldsymbol{\rho}) = (\partial f_i(\boldsymbol{\rho})/\partial \rho_j)_{1\leq i,j\leq N}$ are not available in closed form, so the Riemann problem cannot be solved exactly and numerical schemes that rely on characteristic information become fairly involved (however, these schemes are still competitive in efficiency [7, 16]). Alternatively, one can construct easy-to-implement numerical schemes for (1.1), (1.2) by exploiting the concentration-times-velocity form (1.2) of the fluxes, and utilizing that by (1.3) and (1.4), the functions v_i are non-negative, bounded, and strictly decreasing. These properties were first used in [8] to design a family of relatively simple difference schemes for (1.1), (1.2).

It is the purpose of this work to introduce a new class of schemes for (1.1), (1.2) that do not rely on spectral (characteristic) information and are as easy to implement as the schemes introduced in [8], but perform better in terms of resolution, accuracy and efficiency. To explain the main idea, let us consider the continuity equation for a single driver class ($N = 1$)

$$\partial_t \rho + \partial_x\big(\rho v(\rho)\big) = 0, \quad x \in I, \quad t > 0, \tag{1.5}$$

corresponding to the original LWR model [26, 30], where

$$v(\rho) = v^{\max} V(\rho), \tag{1.6}$$

and for ease of the argument, in the scalar case time is scaled such that $v^{\max}$ equals unity. We formally rewrite (1.5) as

$$\partial_t \rho + \rho \partial_x\big(v(\rho)\big) + v(\rho)\partial_x \rho = 0, \quad x \in I, \quad t > 0. \tag{1.7}$$

The new class of schemes for (1.5) is based on splitting (1.7) into two different equations, which are solved successively for each time iteration. To advance the solution from time t to $t + \Delta t$, we first apply a Lagrangian method [20] to solve

$$\partial_t \rho + \rho \partial_x v(\rho) = 0, \tag{1.8}$$

and use this solution, evolved over the time interval of length Δt, as the initial condition for solving in a second step the transport equation

$$\partial_t \rho + v(\rho)\partial_x \rho = 0, \tag{1.9}$$

whose solution, again evolved over a time interval of length Δt, provides the sought approximate solution valid for $t + \Delta t$. These steps will be identified as "Lagrangian" and "remap" steps, respectively, so the new schemes are addressed as "Lagrangian-remap" (LR) schemes. (The names "Lagrangian" and "remap" will be explained in Sections 3 and 4.)

The idea behind LR schemes is to solve (1.9) using anti-diffusive techniques that have been developed recently for transport equations and thereby to increase the overall efficiency of the proposed splitting strategy, while keeping its simplicity. More precisely, the remap step can be handled in two different ways. One alternative is to employ an anti-diffusive but stable numerical scheme [15] (see also [4, 5]) for the transport equation (1.9) (remap step), where the scheme for the remap step is designed in

such a way that the resulting scheme (first step followed by second step) is conservative. This subclass of LR schemes will be addressed as "Lagrangian-anti-diffusive remap" (L-AR) schemes. The L-AR schemes are discussed in several variants defined by different choices of a particular numerical flux. Alternatively, the remap step can be handled by random sampling in a Glimm-like approach [19]. The resulting scheme, denoted here as "Lagrangian-random-sampling" (L-RS) scheme, is only statistically conservative, but less diffusive than, for example, a (deterministic) integral remap step. Note that the loss of the strict conservativity property does not prevent the convergence to a weak solution in this context.

Both L-AR and L-RS subclasses of LR schemes can readily be extended to the multiple-species case ($N > 1$). For that case, we propose to equip the L-RS scheme with random sampling among the fan of states of the simple Harten, Lax and van Leer (HLL) approximate Riemann solver [25, 32].

Our proposal of the class of LR schemes for the MCLWR model is supported by a partial analysis of the L-AR schemes for $N = 1$, with the conclusion that under suitable CFL conditions, the L-AR schemes have the total variation diminishing (TVD) property and therefore converge to a weak solution and by a number of numerical experiments that show that the proposed schemes are competitive with respect to recent schemes introduced in [8], see Section 2.3.

1.2. Related work. The MCLWR model has been analyzed by several groups of authors, cf. e.g. [3, 16, 27, 37]. In particular, its hyperbolicity has been established [16, 37] and the admissible waves of the Riemann problem have been investigated [37]. Moreover, the model (1.1), (1.2) admits a separable, strictly convex entropy since $\mathcal{J}_{\boldsymbol{f}}(\boldsymbol{\rho})$ is diagonally symmetrizable [2, 3]. Component-wise or characteristic high-resolution numerical schemes for (1.1), (1.2) involving weighted essentially non-oscillatory (WENO) flux reconstructions are advanced in [7, 16, 36]. On the other hand, as mentioned above, particularly simple first- and second-order difference schemes for the same problem that rely on (1.2) along with the definite sign of the velocities v_i are introduced in [8]. Variants of the original MCLWR model [2, 34] have been proposed, and in part analyzed, for highways with varying road surface conditions [9, 38], traffic flow on networks [22, 28], stochastic fundamental diagrams (equivalent to the velocity functions v_i) [29], and diffusive corrections modeling anticipation lengths and reaction times [10].

Anti-diffusive numerical schemes used in this paper have been advanced in the pioneering work by Després and Lagoutière [15] for the linear transport equation with application to gas dynamics, and then extended to monotone scalar conservation laws by Bouchut [5] and applied to Hamilton-Jacobi-Bellman equations by Bokanowski and Zidani in [4]. We refer to [23, 24] and the references therein for further extensions. Variants of the Glimm-like and mixed approach of the L-R and especially L-RS schemes have turned out successful in a number of contexts, ranging from the computation of classical and nonclassical shock waves [11, 12], contacts discontinuities in two-phase flow and traffic flow models [1, 13, 21], to phase transitions in traffic flow models set on a non-convex state space [14].

1.3. Outline of the paper. The remainder of this paper is organized as follows. In Section 2 we state some preliminaries, including the concept of weak and entropy solutions (Section 2.1), some further properties of the MCLWR model (in Section 2.2) and Schemes 4 and 10 of [8] (Section 2.3), which are simple first- and second-order difference schemes that compete with those introduced herein. In Section 3 we describe the discretization of the Lagrangian step, which is based on differencing (1.8)

in Lagrangian coordinates. It is then shown that under appropriate CFL conditions, the resulting scheme for (1.8) satisfies a maximum principle. Next, Section 4 provides a discussion of anti-diffusive schemes to handle the remap step by solving equation (1.9). To this end, in Section 4.1 we introduce the anti-diffusive scheme in general form and identify conditions under which the scheme satisfies an L^∞ bound and is TVD. Then, in Section 4.2, we recall three alternative anti-diffusive numerical fluxes, namely the *limited downwind anti-diffusive flux*, which gives rise to the so-called *UBee* scheme [4]; the *relaxed anti-diffusive flux* of the so-called *r-UBee* scheme [5]; and the flux of the so-called *NBee* scheme introduced in [4]. Then, in Section 4.3, we formulate the L-AR scheme for the complete equation (1.5) and demonstrate that this scheme can be written in conservative form (which is not entirely obvious since (1.8) and (1.9) have been discretized separately). Moreover, we prove that under a suitable CFL condition it satisfies a uniform L^∞ bound and is TVD, and therefore converges to a weak solution of (1.5) as discretization parameters tend to zero. In Section 4.4 we introduce the multi-class ($N > 1$) version of the L-AR scheme and specify the corresponding CFL condition. In Section 5 we introduce the alternative method for solving the remap step, namely the random sampling method. We first consider the scalar case ($N = 1$), which is motivated by the conservative but diffusive integral remap (Section 5.1) and leads to random sampling between two states per cell (Section 5.2). In the multi-class case ($N > 1$), random sampling is done between three states per cell, where the intermediate state is constructed by the approximate HLL Riemann solver, which is recalled in Section 5.3. The complete L-RS method for (1.1) is described in Section 5.4. We emphasize that the L-RS method is not conservative; it is just statistically conservative in the sense that the error in conservation of mass tends to zero as discretization parameters tend to zero.

In Section 6 we present several numerical examples to illustrate the efficiency of the LR schemes for one and several species. In each numerical test we compare the numerical solutions produced by the L-NBee, L-UBee and L-RS schemes with those of Schemes 4 and 10 of [8] (see Section 2.3) to validate our results. Moreover, efficiency plots are presented, and we calculate the total entropy to check numerically whether the numerical solution converges to an entropy solution. Finally, some conclusions are collected in Section 7.

2. Preliminaries.

2.1. Weak solutions and entropy admissibility. We briefly recall the concepts of a weak solution and of entropy for (1.1) under the specific assumptions (1.2) and (1.3), and considering the initial condition

$$\boldsymbol{\rho}(x,0) = \boldsymbol{\rho}_0(x), \quad x \in I. \tag{2.1}$$

We closely follow the preliminary remarks of [9]. First of all, it is well known that even if $\boldsymbol{\rho}_0$ is smooth, solutions of (1.1), (2.1) develop discontinuities, and so we seek a weak solution, which is a bounded measurable function $\boldsymbol{\rho} = \boldsymbol{\rho}(x,t)$ satisfying

$$\int_{\mathbb{R}^+}\int_I \big(\phi_t \boldsymbol{\rho} + \phi_x \boldsymbol{f}(\boldsymbol{\rho})\big)\,\mathrm{d}x\,\mathrm{d}t + \int_I \phi(x,0)\boldsymbol{\rho}_0(x)\,\mathrm{d}x = \mathbf{0} \tag{2.2}$$

for any smooth test function $\phi = \phi(x,t)$ with compact support contained in $I \times \mathbb{R}^+$. If a weak solution $\boldsymbol{\rho}$ has a discontinuity along a smooth curve $x = x(t)$ and $\boldsymbol{\rho}$ is continuous on either side of $x(t)$ with limits $\boldsymbol{\rho}_-$ and $\boldsymbol{\rho}_+$ to the left and right of the

jump, respectively, then the weak formulation (2.2) implies the following Rankine-Hugoniot (RH) jump condition, where $s = \mathrm{d}x/\mathrm{d}t$ is the shock speed:

$$\boldsymbol{f}(\boldsymbol{\rho}_+) - \boldsymbol{f}(\boldsymbol{\rho}_-) = s(\boldsymbol{\rho}_+ - \boldsymbol{\rho}_-). \tag{2.3}$$

Since weak solutions of (1.1) are not unique, an additional admissibility criterion (usually motivated by the "physics" of the problem) needs to be imposed. Suppose that (1.1) admits a strictly convex entropy, i.e. there exists a strictly convex function $\mathcal{E} = \mathcal{E}(\boldsymbol{\rho})$ and an entropy flux $\mathcal{F} = \mathcal{F}(\boldsymbol{\rho})$ such that $\nabla\mathcal{F}(\boldsymbol{\rho}) = \nabla\mathcal{E}(\boldsymbol{\rho})\mathcal{J}_{\boldsymbol{f}}(\boldsymbol{\rho})$. Then a weak solution $\boldsymbol{\rho}$ of (1.1) is said to be *entropy-admissible* [6] if for every smooth nonnegative test function φ with compact support in $I \times (0,\infty)$, the inequality

$$\int_{\mathbb{R}^+}\int_I \big(\varphi_t\mathcal{E}(\boldsymbol{\rho}) + \varphi_x\mathcal{F}(\boldsymbol{\rho})\big)\,\mathrm{d}x\,\mathrm{d}t \geq 0 \tag{2.4}$$

holds. This inequality follows from a parabolic regularization of (1.1) if one lets the regularization parameter tend to zero, assuming that the corresponding solutions converge boundedly a.e. to a limit $\boldsymbol{\rho}$ (cf., e.g., [9, 31]). Note that (2.4) can also be expressed as $\partial_t\mathcal{E}(\boldsymbol{\rho}) + \partial_x\mathcal{F}(\boldsymbol{\rho}) \leq 0$ in the sense of distributions. Moreover, (2.4) implies that all discontinuities satisfy, in addition to (2.3), the entropy jump condition

$$\mathcal{F}(\boldsymbol{\rho}_+) - \mathcal{F}(\boldsymbol{\rho}_-) \leq s\big(\mathcal{E}(\boldsymbol{\rho}_+) - \mathcal{E}(\boldsymbol{\rho}_-)\big). \tag{2.5}$$

For general N and systems of the type (1.1), the existence of an entropy pair $(\mathcal{E}(\boldsymbol{\rho}), \mathcal{F}(\boldsymbol{\rho}))$ that satisfies $\nabla\mathcal{F}(\boldsymbol{\rho}) = \nabla\mathcal{E}(\boldsymbol{\rho})\mathcal{J}_{\boldsymbol{f}}(\boldsymbol{\rho})$ is an exceptional property. However, for the MCLWR model with $\boldsymbol{f}(\boldsymbol{\rho})$ defined by (1.2), (1.3), a convex entropy function $\mathcal{E}(\boldsymbol{\rho})$ and corresponding entropy flux $\mathcal{F}(\boldsymbol{\rho})$ are given by

$$\mathcal{E}(\boldsymbol{\rho}) = \sum_{i=1}^N \frac{\rho_i(\ln\rho_i - 1)}{v_i^{\max}}, \quad \mathcal{F}(\boldsymbol{\rho}) = V(\rho)\sum_{i=1}^N \rho_i\ln\rho_i - \mathcal{V}(\rho), \tag{2.6}$$

where $\mathcal{V}$ is any primitive of V, i.e., $\mathcal{V}'(\rho) = V(\rho)$ (see [2]). Finally, for later use we mention that in [2] it is also shown that for the special choice

$$V(\rho) = 1 - \rho/\rho_{\max}, \tag{2.7}$$

the entropy jump condition (2.5) is equivalent to $\rho_- \leq \rho_+$.

We will not attempt to *prove* that any of the LR schemes converges to an entropy-admissible weak solution. However, further support of the new schemes is provided by a heuristic argument based on evaluating a discrete analogue of $\mathcal{E}(\boldsymbol{\rho})$ for given numerical solutions, and for some examples involving (2.7), we will verify that the numerical solution approximates discontinuities that are consistent with $\rho_- \leq \rho_+$.

2.2. Interlacing property of the MCLWR model. We assume that for $N > 1$, the velocities $v_i^{\max}$ are ordered as $0 < v_1^{\max} \leq v_2^{\max} \leq \cdots \leq v_N^{\max}$. Then the eigenvalues $\lambda_i = \lambda_i(\boldsymbol{\rho})$ interlace with the velocities $v_i = v_i(\rho)$ as follows:

$$v_1 + \sum_{i=1}^N \rho_i v_i^{\max} V'(\rho) \leq \lambda_1 \leq v_1 \leq \cdots \leq v_{j-1} \leq \lambda_j \leq v_j \leq \cdots \leq v_N. \tag{2.8}$$

This property was first proved in [37]. Although the eigenvalues are not available in closed algebraic from, the property (2.8) is useful in that it provides starting values for a numerical root finder, which eventually provides access to the eigenstructure of $\mathcal{J}_{\boldsymbol{f}}(\boldsymbol{\rho})$ and makes the implementation of characteristic-based schemes possible [17]. Finally, note that (2.8) implies that λ_1 may be negative (corresponding to backwards-propagating characteristic information), while always $\lambda_2, \ldots, \lambda_N \geq 0$.

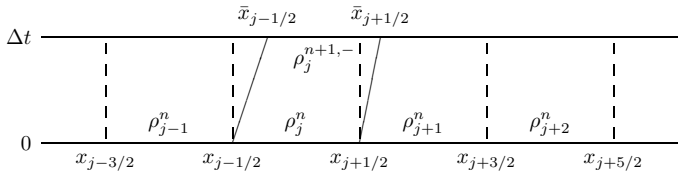

FIG. 3.1. *Illustration of the Lagrangian step.*

2.3. Some simple difference schemes for the MCLWR model. The decisive advantage of our treatment is the simplicity of the new schemes. In that respect these schemes are comparable with a class of schemes introduced in [8]. If $\Delta x = 1/M$ denotes a spatial meshsize, $x_j = j\Delta x$ for $j \in \mathbb{Z}$, $\Delta t > 0$ is a time step, $t^n := n\Delta t$, $\lambda := \Delta t/\Delta x$, and $\rho_{i,j}^n$ denotes the approximate cell average of ρ_i on the cell $[x_{j-1/2}, x_{j+1/2}] \times [t^n, t^{n+1}]$, then Scheme 4 of that paper is defined by

$$\begin{aligned} &\rho_{i,j}^{n+1} = \rho_{i,j}^n - \lambda\big(h_{i,j+1/2}^n - h_{i,j-1/2}^n\big), \\ &h_{i,j+1/2}^n := h_i\big(\boldsymbol{\rho}_j^n, \boldsymbol{\rho}_{j+1}^n\big) := \rho_{i,j}^n v_i\big(\rho_{j+1}^n\big), \quad i = 1, \ldots, N. \end{aligned} \tag{2.9}$$

Scheme 10 of [8] is a version of (2.9) that is second-order accurate both in space and time. It is based on MUSCL-type spatial differencing and Runge-Kutta (RK) time stepping. The MUSCL version of $h_i(\cdot,\cdot)$ is given by

$$h_i^{\mathrm{MUSCL}}\big(\boldsymbol{\rho}_{j-1}^n, \ldots, \boldsymbol{\rho}_{j+2}^n\big) = h_i\left(\boldsymbol{\rho}_{j+1}^n - \frac{1}{2}\boldsymbol{\sigma}_{j+1}^n, \boldsymbol{\rho}_j^n + \frac{1}{2}\boldsymbol{\sigma}_j^n\right), \quad i = 1, \ldots, N,$$

where the "slope vector" $\boldsymbol{\sigma}_j^n := (\sigma_{1,j}^n, \ldots, \sigma_{N,j}^n)^{\mathrm{T}}$ is defined in terms of the van Leer [33] limiter, namely

$$\sigma_{i,j}^n = \frac{|\phi_{i,j}^n - \phi_{i,j-1}^n|(\phi_{i,j+1}^n - \phi_{i,j}^n) + |\phi_{i,j+1}^n - \phi_{i,j}^n|(\phi_{i,j}^n - \phi_{i,j-1}^n)}{|\phi_{i,j}^n - \phi_{i,j-1}^n| + |\phi_{i,j+1}^n - \phi_{i,j}^n|}.$$

Furthermore, if we define the vector $\boldsymbol{h}^{\mathrm{MUSCL}} := (h_1^{\mathrm{MUSCL}}, \ldots, h_N^{\mathrm{MUSCL}})^{\mathrm{T}}$ and

$$\boldsymbol{\Gamma}_j(\boldsymbol{\rho}_{j-2}^n, \ldots, \boldsymbol{\rho}_{j+2}^n) := \lambda\big[\boldsymbol{h}^{\mathrm{MUSCL}}\big(\boldsymbol{\rho}_{j-1}^n, \ldots, \boldsymbol{\rho}_{j+2}^n\big) - \boldsymbol{h}^{\mathrm{MUSCL}}\big(\boldsymbol{\rho}_{j-2}^n, \ldots, \boldsymbol{\rho}_{j+1}^n\big)\big],$$

then Scheme 10 of [8] takes the following two-step form:

$$\tilde{\boldsymbol{\rho}}_j^{n+1} = \tilde{\boldsymbol{\rho}}_j^n - \boldsymbol{\Gamma}_j\big(\boldsymbol{\rho}_{j-2}^n, \ldots, \boldsymbol{\rho}_{j+2}^n\big), \quad \boldsymbol{\rho}_j^{n+1} = \frac{1}{2}\Big(\boldsymbol{\rho}_j^n + \tilde{\boldsymbol{\rho}}_j^{n+1} - \boldsymbol{\Gamma}_j\big(\tilde{\boldsymbol{\rho}}_{j-2}^{n+1}, \ldots, \tilde{\boldsymbol{\rho}}_{j+2}^{n+1}\big)\Big).$$

For the ease of presentation, in the remainder of the paper we will address Schemes 4 and 10 of [8] simply as "Scheme 4" and "Scheme 10", respectively.

3. Discretization of the Lagrangian step. Before introducing a Lagrangian method we observe that defining $\tau := 1/\rho$, we obtain from (1.8) the conservation of mass equation in Lagrangian coordinates

$$\rho\partial_t\tau - \partial_x v = 0. \tag{3.1}$$

In other words, solving (1.8), or equivalently (3.1), means solving the original equation (1.5) on a moving referential mesh with velocity v. Let us then denote $v_{j+1/2}^n$ an approximate value of $v(\rho)$ at the interface point $x = x_{j+1/2}$ at time t^n and assume

now that $\{\rho_j^n\}_{j\in\mathbb{Z}}$ is an approximate solution (1.5) at time $t = t^n$ and used as initial condition for (3.1). Then a numerical solution $\{\rho_j^{n+1,-}\}_{j\in\mathbb{Z}}$ of (3.1) at time Δt can be naturally computed by

$$\rho_j^{n+1,-}\big[\Delta x + \big(v_{j+1/2}^n - v_{j-1/2}^n\big)\Delta t\big] = \rho_j^n \Delta x, \quad j \in \mathbb{Z}, \tag{3.2}$$

since (3.2) expresses that the initial mass in the cell $[x_{j-1/2}, x_{j+1/2}]$ at time t^n (the right-hand side) equals the mass on the modified cell $[\bar{x}_{j-1/2}, \bar{x}_{j+1/2}]$ at time Δt (the left-hand side), where $\bar{x}_{j+1/2} = x_{j+1/2} + v_{j+1/2}^n \Delta t$ are the new interface positions for all j. This is illustrated in Figure 3.1. In particular, with this discretization and using the transformation $\tau_j^n = 1/\rho_j^n$ in (3.2), we obtain the following discretization of (3.1):

$$\rho_j^n\big(\tau_j^{n+1,-} - \tau_j^n\big) = \lambda\big(v_{j+1/2}^n - v_{j-1/2}^n\big).$$

A natural choice for the velocity values in the interface point is $v_{j+1/2} := v(\rho_{j+1}^n)$ for all j. A general theory about Lagrangian schemes can be found in [20].

Now, we indicate some properties of the numerical solution of the Lagrangian scheme (3.2) under certain CFL conditions. The following lemma will be proven for the case of general N, for we use a multi-Lagrangian approach to calculate from $\{\rho_{i,j}^n\}_{i,j}$ the numerical solution of equation (1.8) after an evolution over a time interval of length Δt for each species by

$$\rho_{i,j}^{n+1,-}\big[\Delta x + \big(v_{i,j+1}^n - v_{i,j}^n\big)\Delta t\big] = \rho_{i,j}^n \Delta x, \quad i = 1, \dots, N, \quad j \in \mathbb{Z}. \tag{3.3}$$

LEMMA 3.1. *Assume that the following pair of CFL conditions hold:*

$$\lambda v_i(\rho) \le 1 \quad \text{for } 0 \le \rho \le \rho_{\max}, \tag{3.4}$$

$$-1 \le \lambda \rho_{\max} v_i'(\rho) \le 0 \quad \text{for } 0 \le \rho \le \rho_{\max} \tag{3.5}$$

for all $i = 1, \dots, N$. If $\{\boldsymbol{\rho}_j^{n+1,-}\}_{j\in\mathbb{Z}}$ denotes the numerical solution produced by the scheme (3.2)*, then the following maximum property holds:*

$$0 \le \rho_{i,j}^{n+1,-} \le \max\big\{\rho_j^n, \rho_{j+1}^n\big\} \quad \text{for } i = 1, \dots, N \text{ and all } j \in \mathbb{Z}. \tag{3.6}$$

Proof. The proof depends decisively on the assumption (1.3), so v_i depends only on ρ but not on individual components of $\boldsymbol{\rho}$. The following discussion applies to each index $i \in \{1, \dots, N\}$. Consider first the case $v_{i,j+1}^n \ge v_{i,j}^n$, that is, $\rho_j^n \ge \rho_{j+1}^n$. We then have $\Delta x + (v_{i,j+1}^n - v_{i,j}^n)\Delta t \ge \Delta x$. In this case, (3.3) implies that $\rho_{i,j}^{n+1,-} \le \rho_{i,j}^n \le \rho_j^n$. Since always in the case $v_{i,j+1}^n \ge v_{i,j}^n$ it is clear that $\rho_{i,j}^{n+1,-} \ge 0$, we have thus proved that $0 \le \rho_{i,j}^{n+1,-} \le \rho_j^n$. Consider now the case $v_{i,j+1}^n \le v_{i,j}^n$, that is, $\rho_j^n \le \rho_{j+1}^n$. To establish the upper bound $\rho_{i,j}^{n+1,-} \le \rho_{j+1}^n$, we note that

$$\rho_{i,j}^{n+1,-} = \frac{\rho_{i,j}^n \Delta x}{\Delta x + (v_{i,j+1}^n - v_{i,j}^n)\Delta t} = \frac{\rho_{i,j}^n}{1 + \lambda(v_{i,j+1}^n - v_{i,j}^n)} \le \frac{\rho_j^n}{1 + \lambda(v_{i,j+1}^n - v_{i,j}^n)},$$

so that $\rho_{i,j}^{n+1,-} \le \rho_{j+1}^n$ is proved as soon as one can establish that

$$\frac{\rho_j^n}{1 + \lambda(v_{i,j+1}^n - v_{i,j}^n)} \le \rho_{j+1}^n \Leftrightarrow \big(\rho_{j+1}^n - \rho_j^n\big)\left\{1 + \lambda\rho_{j+1}^n \frac{v_{i,j+1}^n - v_{i,j}^n}{\rho_{j+1}^n - \rho_j^n}\right\} \ge 0.$$

However, the term in curled brackets equals $1 + \lambda\rho_{j+1}^n v_i'(\xi_{j+1/2}^n)$ for an intermediate value $\xi_{j+1/2}^n \in [\rho_j^n, \rho_{j+1}^n]$, and therefore is non-negative under the condition (3.5). ∎

REMARK 3.1. *If $N = 1$ and using similar arguments, (3.6) can be replaced with the more precise estimate* $\min\{\rho_j^n, \rho_{j+1}^n\} \le \rho_{i,j}^{n+1,-} \le \max\{\rho_j^n, \rho_{j+1}^n\}$ *for all $j \in \mathbb{Z}$.*

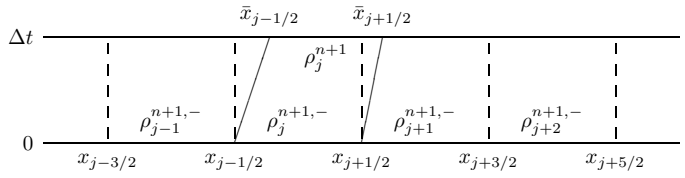

FIG. 4.1. *Illustration of the remap step.*

4. Anti-diffusive schemes for the remap step. After the Lagrangian step, the new values $\rho_j^{n+1,-}$ represent approximate values of the density on a moved mesh with new cells $[\bar{x}_{j-1/2}, \bar{x}_{j+1/2}]$ for all j. To avoid dealing with moving meshes, a so-called remap step is necessary to define the new approximations ρ_j^{n+1} on the uniform mesh with cells $[x_{j-1/2}, x_{j+1/2}]$. Figure 3.1 illustrates that this step amounts to "averaging" the density values at time Δt on the cells $[x_{j-1/2}, x_{j+1/2}]$. Clearly, this average step can equivalently be reformulated by the solution of the transport equation (1.9) with initial data defined by $\rho_j^{n+1,-}$ on each cell $[x_{j-1/2}, x_{j+1/2}]$, see Figure 4.1. The aim of this section is to propose and investigate several discretizations of (1.9), whereby we seek to introduce as little numerical diffusion as possible.

4.1. Anti-diffusive schemes. Here, we describe the conditions analyzed in [15] (see also [4, 5]) for solving (1.9) with initial condition $\{\rho_j^{n+1,-}\}_{j\in\mathbb{Z}}$ by using an anti-diffusive numerical scheme in the form

$$\rho_j^{n+1} = \rho_j^{n+1,-} - \bar{V}_j^n \lambda\big(\rho_{j+1/2}^{n+1,-} - \rho_{j-1/2}^{n+1,-}\big), \quad j \in \mathbb{Z}. \tag{4.1}$$

Here $\bar{V}_j^n$ is a velocity value, defined in terms of available density values, which will be chosen in such a way that the whole scheme (3.2), (4.1) is conservative. The quantities $\rho_{j+1/2}^{n+1,-}$ are numerical fluxes associated with the cell interfaces $x_{j+1/2}$, and will be chosen such that the scheme (4.1) has certain stability and consistency properties.

The construction of the scheme, and some basic results, are identical for the scalar ($N = 1$) and multi-class ($N > 1$) cases. We will therefore consider the corresponding scheme for general N: anti-diffusive numerical scheme, which includes (4.1) for $N = 1$:

$$\rho_{i,j}^{n+1} = \rho_{i,j}^{n+1,-} - \bar{V}_{i,j}^n \lambda\big(\rho_{i,j+1/2}^{n+1,-} - \rho_{i,j-1/2}^{n+1,-}\big), \quad i = 1, \dots, N, \quad j \in \mathbb{Z}. \tag{4.2}$$

Next, we define the quantities

$$\begin{aligned}
&m_{i,j-1/2} := \min\big\{\rho_{i,j}^{n+1,-}, \rho_{i,j-1}^{n+1,-}\big\}, \quad M_{i,j-1/2} := \max\big\{\rho_{i,j}^{n+1,-}, \rho_{i,j-1}^{n+1,-}\big\},\\
&b_{i,j}^+ := M_{i,j-1/2} + \frac{\rho_{i,j}^{n+1,-} - M_{i,j-1/2}}{\max\{v_{i,j}^n, v_{i,j+1}^n\}\lambda}, \quad B_{i,j}^+ := m_{i,j-1/2} + \frac{\rho_{i,j}^{n+1,-} - m_{i,j-1/2}}{\max\{v_{i,j}^n, v_{i,j+1}^n\}\lambda},\\
&a_{i,j+1/2} := \max\big\{b_{i,j}^+, m_{i,j+1/2}\big\}, \quad A_{i,j+1/2} := \min\big\{B_{i,j}^+, M_{i,j+1/2}\big\}.
\end{aligned}$$

According to [15], to ensure the consistency property

$$\rho_{i,j+1/2}^{n+1,-} \to \rho_i \quad \text{as } \rho_{i,j}^{n+1,-}, \rho_{i,j+1}^{n+1,-} \to \rho_i, \quad 0 \le \rho_i \le \rho_{\max}, \quad i = 1, \dots, N, \quad j \in \mathbb{Z},$$

it is sufficient that

$$m_{i,j+1/2} \le \rho_{i,j+1/2}^{n+1,-} \le M_{i,j+1/2} \quad \text{for all } j \in \mathbb{Z}, \tag{4.3}$$

while for the L^∞ and TVD stability conditions it is necessary to have

$$b^+_{i,j} \le \rho^{n+1,-}_{i,j+1/2} \le B^+_{i,j} \quad \text{for all } j \in \mathbb{Z}. \tag{4.4}$$

For the definition of the flux $\rho^{n+1,-}_{i,j+1/2}$, note that the choice

$$\rho^{n+1,-}_{i,j+1/2} = \rho^{n+1,-}_{i,j} \quad \text{for all } j \in \mathbb{Z} \tag{4.5}$$

produces a diffusive and stable scheme, while $\rho^{n+1,-}_{i,j+1/2} = \rho^{n+1,-}_{i,j+1}$ for all $j \in \mathbb{Z}$ yields an anti-diffusive but unstable scheme. For this reason, Després and Lagoutière [15] proposed to choose $\rho^{n+1,-}_{i,j+1/2}$ as close to the value $\rho^{n+1,-}_{i,j+1}$ as possible, subject to the constraints (4.3) and (4.4). In Section 4.2 we discuss how to choose this numerical flux. In the following lemma, the first part of which is proved in [15] and extended to the case of nonlinear conservation laws by Bouchut [5], we resume the existence and properties of the schemes defined by (4.1). Moreover, for $a_1, a_2, \dots, a_m \in \mathbb{R}$ we define the interval $\mathcal{I}(a_1, \dots, a_m) := [\min\{a_1, \dots, a_m\}, \max\{a_1, \dots, a_m\}]$.

LEMMA 4.1. *Assume that the condition* (3.4) *is in effect. Then*

$$a_{i,j+1/2} \le \rho^{n+1,-}_{i,j} \le A_{i,j+1/2} \quad \text{for all } j \in \mathbb{Z},$$

and for any flux that satisfies

$$\rho^{n+1,-}_{i,j+1/2} \in [a_{i,j+1/2}, A_{i,j+1/2}] \quad \text{for all } j \in \mathbb{Z}, \tag{4.6}$$

the scheme (4.2) *is L^∞-stable and TVD, i.e.*

$$\rho^{n+1}_{i,j} \in \mathcal{I}\big(\rho^{n+1,-}_{i,j-1}, \rho^{n+1,-}_{i,j}\big) \quad \text{for all } j \in \mathbb{Z}, \tag{4.7}$$

$$\sum_{j\in\mathbb{Z}} \big|\rho^{n+1}_{i,j+1} - \rho^{n+1}_{i,j}\big| \le \sum_{j\in\mathbb{Z}} \big|\rho^{n+1,-}_{i,j+1} - \rho^{n+1,-}_{i,j}\big| \quad \text{for } n \in \mathbb{N}_0. \tag{4.8}$$

In particular, for each i, j and n there exist numbers $\alpha_{i,j} \in [0,1]$ such that

$$\rho^{n+1,-}_{i,j} = \alpha_{i,j}\rho^{n+1,-}_{i,j-1/2} + (1-\alpha_{i,j})\rho^{n+1,-}_{i,j+1/2}. \tag{4.9}$$

Proof. In [15] the properties (4.7) and (4.8) are proved. We only prove property (4.9). To this end, assume that (3.4) is in effect and that $\rho^{n+1,-}_{i,j+1/2}$ satisfies (4.3) and (4.4). If $\rho^{n+1,-}_{i,j} = M_{i,j-1/2}$, then (4.4) implies that

$$\rho^{n+1,-}_{i,j} \le \rho^{n+1,-}_{i,j+1/2} \le \max\big\{\rho^{n+1,-}_{i,j-1/2}, \rho^{n+1,-}_{i,j+1/2}\big\}. \tag{4.10}$$

On the other hand, from (4.3) we have $\rho^{n+1,-}_{i,j-1/2} \le M_{i,j-1/2} = \rho^{n+1,-}_{i,j}$, and thus

$$\min\big\{\rho^{n+1,-}_{i,j-1/2}, \rho^{n+1,-}_{i,j+1/2}\big\} \le \rho^{n+1,-}_{i,j}. \tag{4.11}$$

Combining (4.10) and (4.11) we obtain $\rho^{n+1,-}_{i,j} \in \mathcal{I}(\rho^{n+1,-}_{j-1/2}, \rho^{n+1,-}_{j+1/2})$, which implies (4.9). The proof is similar if $\rho^{n+1,-}_{i,j} = m_{i,j-1/2}$. ∎

REMARK 4.1. *From* (4.7) *in Lemma 4.1 and the lower bound* (3.6) *of Lemma 3.1 we obtain that $\rho^{n+1}_{i,j} \ge 0$ for all $j \in \mathbb{Z}$.*

4.2. Choice of the numerical fluxes. We have specified in Section 4.1 the stability bounds (4.6) for the numerical fluxes that guarantee that the whole L-AR scheme (4.13) converges to a weak solution of (1.5). Following the methodology outlined in [15] (see also [5, 4, 35]), we now describe numerical techniques for solving (1.9) by an anti-diffusive scheme in the form (4.1). Since the choice (4.5) leads to a stable but diffusive scheme, we choose the numerical flux $\rho^{n+1,-}_{j+1/2}$ as close as possible to the downwind value $\rho^{n+1,-}_{j+1}$ under the CFL condition (3.4).

4.2.1. Limited downwind anti-diffusive flux. This numerical flux was formulated by Després and Lagoutière [15] and is defined by

$$\rho_{j+1/2}^{n+1,-} := \operatorname*{argmin}_{\rho\in[a_{j+1/2},A_{j+1/2}]} \left|\rho-\rho_{j+1}^{n+1,-}\right| = \min\bigl\{\max\bigl\{\rho_{j+1}^{n+1,-},a_{j+1/2}\bigr\},A_{j+1/2}\bigr\}.$$

In Lemma 4.1 it is proved that this scheme satisfies (4.6). Following [4] we denote this scheme for (1.9) by *UBee*, and refer to the corresponding complete L-AR scheme as *L-UBee* scheme.

4.2.2. Relaxed anti-diffusive flux. An equivalent form of the UBee scheme was formulated by Bouchut [5] for the advection equation as follows:

$$\rho_{j+1/2}^{n+1,-} := \rho_{j+1/2}^{\mathrm{diss}} + \operatorname{minmod}\bigl(\rho_{j+1/2}^{\mathrm{L}}-\rho_{j+1/2}^{\mathrm{diss}},\rho_{j+1/2}^{\mathrm{R}}-\rho_{j+1/2}^{\mathrm{diss}}\bigr),$$

where the standard minmod function is defined by

$$\operatorname{minmod}(a,b) := \begin{cases} \operatorname{sgn}(a)\min\{|a|,|b|\} & \text{if } \operatorname{sgn}a=\operatorname{sgn}b,\\ 0 & \text{otherwise,}\end{cases}$$

the dissipative flux $\rho_{j+1/2}^{\mathrm{diss}}$ is the classical upwind flux, and $\rho_{j+1/2}^{\mathrm{L}}$ and $\rho_{j+1/2}^{\mathrm{R}}$ are the extremal left-wind and right-wind fluxes. These quantities are defined as follows:

$$\rho_{j+1/2}^{\mathrm{diss}} = \rho_j^{n+1,-},\quad \rho_{j+1/2}^{\mathrm{L}} = \frac{\rho_j^{n+1,-}-\rho_{j-1}^{n+1,-}}{\lambda\max\{v_j^n,v_{j+1}^n\}}+\rho_{j-1}^{n+1,-},\quad \rho_{j+1/2}^{\mathrm{R}} = \rho_{j+1}^{n+1,-}.$$

A modification described in [35] for the advection equation consists in applying a relaxed anti-diffusive flux as follows:

$$\rho_{j+1/2}^{n+1,-} := \rho_{j+1/2}^{\mathrm{diss}} + \varphi_j\operatorname{minmod}\bigl(\rho_{j+1/2}^{\mathrm{L}}-\rho_{j+1/2}^{\mathrm{diss}},\rho_{j+1/2}^{\mathrm{R}}-\rho_{j+1/2}^{\mathrm{diss}}\bigr).$$

Here $\varphi_j\in[0,1]$ is a discontinuity indicator with $\varphi_j\approx 0$ in smooth regions and $\varphi_j\approx 1$ near a discontinuity. Such a choice of φ_j guarantees that (4.6) is satisfied. We denote this scheme for (1.9) by *rUBee*, and the corresponding L-AR scheme by *L-rUBee* scheme. The discontinuity indicator is chosen as $\varphi_j=\beta_j/(\beta_j+\gamma_j)$, where

$$\mu_j = \left|\rho_{j-1}^{n+1,-}-\rho_j^{n+1,-}\right|^2+\varepsilon,\quad \beta_j = \left|\frac{\mu_j}{\mu_{j-1}}+\frac{\mu_{j+1}}{\mu_{j+2}}\right|^2,\quad \gamma_j = \frac{|\rho_{\max}^{n+1,-}-\rho_{\min}^{n+1,-}|^2}{\mu_j},$$

where $\rho_{\max}^{n+1,-}$ and $\rho_{\min}^{n+1,-}$ are the maximum and minimum values of $\rho_j^{n+1,-}$ for all grid points, ε is a small positive number taken as $\varepsilon=10^{-6}$. Clearly, $0\le\mu_j\le 1$. Near a discontinuity, $\gamma_j\ll\beta_j$, so $\varphi_j\approx 1$, and $\varphi_j=O(\Delta x^2)$ in smooth regions.

4.2.3. NBee scheme. This scheme, which was proposed by Bokanowski and Zidani in [4] for linear transport equations, corresponds to a second-order scheme in space which is more diffusive than the U-Bee scheme, and which is defined by

$$\rho_{j+1/2}^{n+1,-} := \rho_j^{n+1,-}+\frac{1-\bar\lambda}{2}\varphi_j\bigl(\rho_{j+1}^{n+1,-}-\rho_j^{n+1,-}\bigr), \tag{4.12}$$

where $\bar\lambda=\lambda\max\{v_j^n,v_{j+1}^n\}$ and $\varphi_j=\varphi^{\mathrm{NB}}(r_j,\bar\lambda)$, where

$$r_j := \frac{\rho_j^{n+1,-}-\rho_{j-1}^{n+1,-}}{\rho_{j+1}^{n+1,-}-\rho_j^{n+1,-}},\quad \varphi^{\mathrm{NB}}(r,\bar\lambda) := \max\left\{0,\min\left\{1,\frac{2r}{\bar\lambda}\right\},\min\left\{r,\frac{2}{1-\bar\lambda}\right\}\right\}.$$

It is proved in [4] that the numerical flux (4.12) satisfies the assumptions of Lemma 4.1. This so-called NBee scheme (for (1.9)) is written here in a limiter version. We refer to the corresponding L-AR scheme as *L-NBee* scheme.

4.3. Lagrangian-anti-diffusive remap (L-AR) schemes, scalar case ($N = 1$). We are now able to describe the subclass of Lagrangian-anti-diffusive remap (L-AR) schemes of LR schemes. Assume we have a numerical solution $\{\rho_j^n\}_{j\in\mathbb{Z}}$ that approximate the solution of (1.5) at time $t = t^n$ and wish to advance this solution to $t = t^{n+1} = t^n + \Delta t$, where Δt is subject to certain CFL-type restrictions. To this end, two steps are performed successively:

1. *Lagrangian step.* Consider that $\{\rho_j^n\}_{j\in\mathbb{Z}}$ is an initial solution for (1.8). Then we can obtain a numerical solution $\{\rho_j^{n+1,-}\}_{j\in\mathbb{Z}}$ after an evolution over a time interval of length Δt, by using scheme (3.2).
2. *Anti-diffusive remap step.* Solve (1.9) with initial condition $\{\rho_j^{n+1,-}\}_{j\in\mathbb{Z}}$ using an anti-diffusive scheme (4.1) for a specific choice of $\bar{V}_j^n$, obtaining a numerical solution $\{\rho_j^{n+1}\}_{j\in\mathbb{Z}}$ which approximates the solution of (1.5) at time $t = t^{n+1}$.

In the next theorem, the choice of $\bar{V}_j^n$ is motivated by the existence of a classical conservative update formula for the whole LR scheme (3.2), (4.1).

THEOREM 4.1. *Assume that the CFL conditions* (3.4) *and* (3.5) *are satisfied. Then there exists a definition of* $\bar{V}_j^n \in \mathcal{I}(v_j^n, v_{j+1}^n)$ *such that the complete L-AR scheme can be written in the form*

$$\rho_j^{n+1} = \rho_j^n - \lambda\big(\rho_{j+1/2}^{n+1,-} v_{j+1}^n - \rho_{j-1/2}^{n+1,-} v_j^n\big), \quad j \in \mathbb{Z}, \quad n \in \mathbb{N}_0. \tag{4.13}$$

Proof. Let $\{\rho_j^{n+1,-}\}_{j\in\mathbb{Z}}$ be a solution of (1.8) obtained by numerical scheme (3.2). Using this solution we solve equation (1.9) by the scheme (4.1), where the value $\bar{V}_j^n$ still needs to be determined in such a way that the resulting scheme is conservative. Replacing $\rho_j^{n+1,-}$ in (4.1) by $\rho_j^{n+1,-} = \rho_j^n - \lambda(v_{j+1}^n - v_j^n)\rho_j^{n+1,-}$, we obtain

$$\rho_j^{n+1} = \rho_j^n - \lambda\bar{V}_j^n\big(\rho_{j+1/2}^{n+1,-} - \rho_{j-1/2}^{n+1,-}\big) - \lambda\big(v_{j+1}^n - v_j^n\big)\rho_j^{n+1,-}. \tag{4.14}$$

Since $\rho_{j+1/2}^{n+1,-}$ satisfies the assumptions of Lemma 4.1, (4.9) implies that there exist numbers $\alpha_j^n \in [0,1]$ such that $\rho_j^{n+1,-} = \alpha_j^n \rho_{j-1/2}^{n+1,-} + (1-\alpha_j^n)\rho_{j+1/2}^{n+1,-}$ for $j \in \mathbb{Z}$, i.e. we may define

$$\alpha_j^n = \begin{cases} \dfrac{\rho_j^{n+1,-} - \rho_{j+1/2}^{n+1,-}}{\rho_{j-1/2}^{n+1,-} - \rho_{j+1/2}^{n+1,-}} & \text{if } \rho_{j-1/2}^{n+1,-} - \rho_{j+1/2}^{n+1,-} \neq 0, \\ 0 & \text{otherwise.} \end{cases}$$

With α_j^n defined in this way, we set $\bar{V}_j^n := (1-\alpha_j^n)v_j^n + \alpha_j^n v_{j+1}^n$, and replacing in equation (4.14) we obtain (4.13). ∎

REMARK 4.2. *(Important) From a practical point of view, the L-AR schemes are implemented by simply using the equivalent form* (4.13)*. From a theoretical point of view, the Lagrangian-remap decomposition of* (4.13) *is used to prove the stability properties in theorem 4.2 below, using Lemmas 3.1 and 4.1 for the Lagrangian and remap steps, respectively.*

Note that the numerical scheme (4.13) is written conservative form

$$\rho_j^{n+1} = \rho_j^n - \lambda\big(F_{j+1/2}^n - F_{j-1/2}^n\big),$$

where $F_{j+1/2}^n := F(\rho_{j-1}^n, \dots, \rho_{j+2}^n) := \rho_{j+1/2}^{n+1,-} v_{j+1}^n$ denotes the numerical flux. This four-point numerical flux is consistent with the flux $f(\rho) = \rho v(\rho)$ since by (3.2) and (4.3), we have $\rho_{j-1}^{n+1,-}, \rho_j^{n+1,-}, \rho_{j+1}^{n+1,-} \to \rho$ as $\rho_{j-1}^n, \dots, \rho_{j+2}^n \to \rho$. This eventually means that $F(\rho, \dots, \rho) = \rho v(\rho)$.

Next, we prove some properties for the numerical scheme (4.13).

THEOREM 4.2. *Assume that the CFL conditions* (3.4) *and* (3.5) *are satisfied. Then the numerical scheme* (4.13) *has the TVD property, is L^∞-stable, and as consequence of* (3.6) *and* (4.7) *it satisfies $\rho_j^{n+1} \in \mathcal{I}(\rho_{j-1}^n, \rho_j^n, \rho_{j+1}^n)$ for all $j \in \mathbb{Z}$ and $n \in \mathbb{N}_0$.*

Proof. We recall from Lemma 4.1 that if (3.4) is satisfied and the scheme associated with the remap step, (4.1), satisfies (4.6), then (4.1) has the TVD property (4.8). For the Lagrangian step, we obtain from (3.2)

$$\begin{aligned}\rho_{j+1}^{n+1,-} - \rho_j^{n+1,-} = &\big[1 + \lambda\rho_j^{n+1,-} v'\big(\zeta_{j+1/2}^n\big)\big]\big(\rho_{j+1}^n - \rho_j^n\big)\\ &- \lambda\rho_{j+1}^{n+1,-} v'\big(\zeta_{j+3/2}\big)\big(\rho_{j+3/2}^n - \rho_{j+1}^n\big).\end{aligned} \tag{4.15}$$

Since $\rho_j^{n+1,-} \geq 0$, $v'(\rho) \leq 0$ and $1 + \lambda\rho_j^{n+1,-} v'(\zeta_{j+1/2}^n) \geq 1 + \lambda\rho_{\max} v'(\zeta_{j+1/2}^n) \geq 0$ due to the CFL condition (3.5), (4.15) implies that

$$\begin{aligned}\big|\rho_{j+1}^{n+1,-} - \rho_j^{n+1,-}\big| \leq &\big[1 + \lambda\rho_j^{n+1,-} v'\big(\zeta_{j+1/2}^n\big)\big]\big|\rho_{j+1}^n - \rho_j^n\big|\\ &- \lambda\rho_{j+1}^{n+1,-} v'\big(\zeta_{j+3/2}^n\big)\big|\rho_{j+2}^n - \rho_{j+1}^n\big| \quad \text{for all } j \in \mathbb{Z}.\end{aligned}$$

Summing over $j \in \mathbb{Z}$, we get

$$\begin{aligned}\sum_{j\in\mathbb{Z}}\big|\rho_{j+1}^{n+1,-} - \rho_j^{n+1,-}\big| \leq &\sum_{j\in\mathbb{Z}}\big|\rho_{j+1}^n - \rho_j^n\big| + \lambda\sum_{j\in\mathbb{Z}}\rho_j^{n+1,-} v'\big(\zeta_{j+1/2}^n\big)\big|\rho_{j+1}^n - \rho_j^n\big|\\ &- \lambda\sum_{j\in\mathbb{Z}}\rho_{j+1}^{n+1,-} v'\big(\zeta_{j+3/2}^n\big)\big|\rho_{j+2}^n - \rho_{j+1}^n\big|\\ = &\sum_{j\in\mathbb{Z}}|\rho_{j+1}^n - \rho_j^n|.\end{aligned} \tag{4.16}$$

Then, from (4.8) and (4.16) we obtain the TVD property for the numerical scheme (4.13) under the natural CFL conditions (3.4) and (3.5). The L^∞ bound is a consequence of the TVD property, i.e.,

$$\big|\rho_j^{n+1}\big| \leq \sum_{m=-\infty}^{j}\big|\rho_m^{n+1} - \rho_{m-1}^{n+1}\big| \leq \sum_{j\in\mathbb{Z}}\big|\rho_{j+1}^{n+1} - \rho_j^{n+1}\big| \leq \sum_{j\in\mathbb{Z}}\big|\rho_{j+1}^0 - \rho_j^0\big|.$$

□

REMARK 4.3. *A consequence of Theorem 4.2 is that under CFL conditions* (3.4) *and* (3.5) *if $\rho_0 \in L^1(\mathbb{R})$, the numerical solution of scheme* (4.13) *converges in $L^\infty([0,T], L^1_{\mathrm{loc}})$ to a weak solution of* (1.5)*, see [20].*

4.4. The multi-species case ($N \geq 1$) and CFL condition. First of all, also in the multi-species case the complete L-AR scheme admits a conservative update formula. The following lemma can be proved in the same way as Theorem 4.1:

LEMMA 4.2. *Assume that* (3.4) *and* (3.5) *is valid, then there exists a definition of $\bar{V}_{i,j}^n \in \mathcal{I}(v_{i,j}^n, v_{i,j+1}^n)$ such that the complete L-AR scheme can be written in the following component-wise version of* (4.13)*:*

$$\rho_{i,j}^{n+1} = \rho_{i,j}^n - \lambda\big(\rho_{i,j+1/2}^{n+1,-} v_{i,j+1}^n - \rho_{i,j-1/2}^{n+1,-} v_{i,j}^n\big), \quad i = 1,\dots,N, \quad j \in \mathbb{Z}, \quad n \in \mathbb{N}_0. \tag{4.17}$$

With respect to the CFL condition, inequalities (3.4) and (3.5) are conditions to guarantee positivity, TVD property and maximum principle for numerical solution of scalar conservation laws by is not generally hold in the system case. Below we derive the form of a CFL condition by requiring that a certain invariant region be preserved. This invariant region is defined as

$$\mathcal{D}_{\rho_{\max}} := \big\{(\rho_1,\dots,\rho_N)^{\mathrm{T}} \in \mathbb{R}^N : \rho_1 \geq 0,\dots,\rho_N \geq 0,\, \rho = \rho_1 + \cdots + \rho_N \leq \rho_{\max}\big\}.$$

THEOREM 4.3. *Consider the numerical scheme* (4.17) *where the velocity functions are defined as* (1.3) *with* $v_1^{\max} < \cdots < v_N^{\max}$ *and the hindrance factor* $V(\rho)$ *satisfies* (1.4). *If* $\boldsymbol{\rho}_j^n \in \mathcal{D}_{\rho_{\max}}$ *for* $j \in \mathbb{Z}$ *and the (strengthened) CFL conditions*

$$\lambda v_N^{\max} \leq 1, \quad \lambda \rho_{\max} N v_N^{\max} \max_{0\leq\rho\leq\rho_{\max}} |V'(\rho)| \leq 1 \tag{4.18}$$

are satisfied at time level n, *then* $\boldsymbol{\rho}_j^{n+1} \in \mathcal{D}_{\rho_{\max}}$ *for* $j \in \mathbb{Z}$.

Proof. Suppose that $\boldsymbol{\rho}_j^n \in \mathcal{D}_{\rho_{\max}}$. Then we obtain that $\rho_{i,j}^{n+1} \geq 0$ for $i = 1,\dots,N$ and $j \in \mathbb{Z}$ (cf. Remark 4.1). On the other hand, since also $\rho_{i,j+1/2}^{n+1,-} \geq 0$ for all $i = 1,\dots,N$ and $j \in \mathbb{Z}$, thanks to the conservative update formula (4.17) we can write $0 \leq \rho_{i,j}^{n+1} \leq \rho_{i,j}^n + \lambda \rho_{i,j-1/2}^{n+1,-} v_{i,j}^n$ for $i = 1,\dots,N$ and $j \in \mathbb{Z}$, and then

$$0 \leq \rho_{i,j}^{n+1} \leq \rho_{i,j}^n + \lambda \rho_{i,j-1/2}^{n+1,-} v_N^{\max} V\big(\rho_j^n\big), \quad i = 1,\dots,N, \quad j \in \mathbb{Z}. \tag{4.19}$$

Summing (4.19) over $i = 1,\dots,N$ we get

$$0 \leq \rho_j^{n+1} \leq \rho_j^n + \lambda v_N^{\max} V\big(\rho_j^n\big)\big(\rho_{1,j-1/2}^{n+1,-} + \cdots + \rho_{N,j-1/2}^{n+1,-}\big). \tag{4.20}$$

But by (4.10) and Lemma 3.1, $\rho_{i,j-1/2}^{n+1,-} \leq \max\{\rho_{j-1}^{n+1,-}, \rho_j^{n+1,-}\} \leq \rho_{\max}$. Then we get from (4.20) $0 \leq \rho_j^{n+1} \leq \rho_j^n + \lambda N v_N^{\max} V(\rho_j^n)\rho_{\max} =: G(\rho_j^n)$. Assumption (1.4) implies that $G(\rho_{\max}) = \rho_{\max}$, and since $G'(\rho_j^n) = 1 + \lambda \rho_{\max} v_N^{\max} V'(\rho_j^n)$, the second CFL condition in (4.18) implies that $\rho \mapsto G(\rho)$ is an increasing function. Thus, $\max_{0\leq\rho_j^n\leq\rho_{\max}} G(\rho_j^n) = \rho_{\max}$, implying that $\rho_j^{n+1} \leq \rho_{\max}$. ∎

5. Statistically conservative schemes. We now introduce an alternative for solving the remap step in the one-species or multi-species cases to recover updated values of the unknown on the initial mesh.

5.1. Integral remap. For the scalar case ($N = 1$), if $\{\rho_j^{n+1,-}\}_{j\in\mathbb{Z}}$ is the numerical solution given by (3.2), we set

$$\rho^{n+1,-}(x) := \sum_{j\in\mathbb{Z}} \rho_j^{n+1,-} \chi_{[\bar{x}_{j-1/2},\bar{x}_{j+1/2}]}(x).$$

To define the new approximation ρ_j^{n+1} on the uniform mesh with cells $[x_{j-1/2}, x_{j+1/2}]$ at time t^{n+1}, one could be tempted to apply an integral remap

$$\rho_j^{n+1} := \frac{1}{\Delta x} \int_{x_{j-1/2}}^{x_{j+1/2}} \rho^{n+1,-}(x)\,\mathrm{d}x, \quad j \in \mathbb{Z}.$$

After some calculations one obtains

$$\Delta x \rho_j^{n+1} = (\bar{x}_{j-1/2} - x_{j-1/2})\rho_{j-1}^{n+1,-} + (x_{j+1/2} - \bar{x}_{j-1/2})\rho_j^{n+1,-},$$

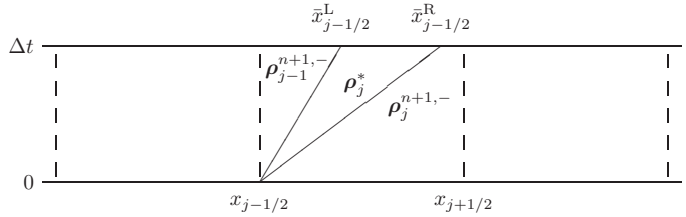

FIG. 5.1. *Illustration of the function* $(x,t) \to \tilde{\boldsymbol{\rho}}(x,t)$ *with* $\bar{x}^{\mathrm{L,R}}_{j-1/2} := x_{j-1/2} + \sigma_{\mathrm{L,R}}\Delta t$.

which yields

$$\rho_j^{n+1} = \lambda v_j^n \rho_{j-1}^{n+1,-} + \big(1 - \lambda v_j^n\big)\rho_j^{n+1,-}. \tag{5.1}$$

According to the definition (3.2), a complete scheme for Lagrangian step plus remap step can be written in the form

$$\rho_j^{n+1} = \rho_j^n - \lambda\big(v_{j+1}^n \rho_j^{n+1,-} - v_j^n \rho_{j-1}^{n+1,-}\big). \tag{5.2}$$

As consequence of (5.1) and Lemma 3.1, under a CFL condition (3.4) and (3.5), the numerical scheme (5.2) is conservative, TVD, L^∞-stable and satisfies the maximum principle. However, let us emphasize that it is not our intention to use this alternative since such an average formula (5.1) produces too much numerical diffusion.

5.2. Random sampling remap, scalar case ($N = 1$). In order to define ρ_j^{n+1} without introducing numerical diffusion, we follow a Glimm-type random sampling strategy [19]. More precisely, for given well-distributed random sequence $\{a_n\}_{n\in\mathbb{N}}$ taking values in $(0,1)$ (e.g. the Van der Corput sequence, cf. [32, Sect. 7.5.1]), we simply set

$$\rho_j^{n+1} = \begin{cases} \rho_{j-1}^{n+1,-} & \text{if } a_{n+1} \in (0, \lambda v_j^n), \\ \rho_j^{n+1,-} & \text{if } a_{n+1} \in (\lambda v_j^n, 1). \end{cases} \tag{5.3}$$

A CFL condition obtained from (5.3) is $\lambda v(\rho) \le 1, \quad 0 \le \rho \le \rho_{\max}$.

5.3. Random sampling remap, multi-class case ($N > 1$). For the multi-species cases, first, we calculate $\boldsymbol{\rho}_j^{n+1,-} = (\rho_{1,j}^{n+1,-}, \dots, \rho_{N,j}^{n+1,-})^{\mathrm{T}}$ by applying the multi-Lagrangian formula (3.3). One first idea to define the new approximation $\boldsymbol{\rho}_j^{n+1}$ by a multi-species version of formula (5.3), but numerical experiments show that this strategy generates spurious oscillations that do not disappear with the refinement. The strategy to avoid this undesirable behaviour is to use the approximate HLL Riemann solver to locally obtain an intermediate value limited by the curves generated for the extremal maximum velocities. It consists in redefining the numerical solution $\tilde{\boldsymbol{\rho}}(x,t)$ of the Lagrangian step in the region $[x_{j-1/2}, x_{j+1/2}] \times [0, \Delta t]$ by

$$\tilde{\boldsymbol{\rho}}(x,t) = \begin{cases} \boldsymbol{\rho}_{j-1}^{n+1,-} & \text{if } (x - x_{j-1/2})/t < \sigma_{\mathrm{L}}, \\ \boldsymbol{\rho}_j^{*} & \text{if } \sigma_{\mathrm{L}} < (x - x_{j-1/2})/t < \sigma_{\mathrm{R}}, \\ \boldsymbol{\rho}_j^{n+1,-} & \text{if } (x - x_{j-1/2})/t > \sigma_{\mathrm{R}}, \end{cases} \tag{5.4}$$

see Figure 5.1. Here $\sigma_{\mathrm{L}} = v_1^{\max} V(\boldsymbol{\rho}_j^n)$ and $\sigma_{\mathrm{R}} = v_N^{\max} V(\boldsymbol{\rho}_j^n)$ are the extremal maximum velocities, and the state $\boldsymbol{\rho}_j^*$ is calculated according to the consistency relation

$$v_i(\boldsymbol{\rho}_j^n)\big(\rho_{i,j}^{n+1,-} - \rho_{i,j-1}^{n+1,-}\big) = \sigma_{\mathrm{L}}\big(\rho_{i,j}^{*} - \rho_{i,j-1}^{n+1,-}\big) + \sigma_{\mathrm{R}}\big(\rho_{i,j}^{n+1,-} - \rho_{i,j}^{*}\big), \quad i = 1, \dots, N.$$

This relation is consistent with the integral form of the system of equations

$$\partial_t \rho_i + v_i(\boldsymbol{\rho})\partial_x \rho_i = 0, \quad i = 1, \dots, N \tag{5.5}$$

over the control volume $[x_{\rm L}, x_{\rm R}] \times [0, \Delta t]$ where $x_{\rm L} \le \Delta t \sigma_{\rm L}$ and $x_{\rm R} \ge \Delta t \sigma_{\rm R}$ [32].

Here, we use relation (5.4) to define an anti-diffusive scheme to update the numerical value $\boldsymbol{\rho}_j^{n+1}$, namely we set

$$\boldsymbol{\rho}_j^{n+1} = \begin{cases} \boldsymbol{\rho}_{j-1}^{n+1,-} & \text{if } a_{n+1} \in (0, \lambda\sigma_{\rm L}), \\ \boldsymbol{\rho}_j^{*} & \text{if } a_{n+1} \in (\lambda\sigma_{\rm L}, \lambda\sigma_{\rm R}), \\ \boldsymbol{\rho}_j^{n+1,-} & \text{if } a_{n+1} \in (\lambda\sigma_{\rm R}, 1). \end{cases} \tag{5.6}$$

A CFL condition obtained from (5.6) is

$$\lambda v_N^{\max} V(\rho) \le 1, \quad 0 \le \rho \le \rho_{\max}, \quad i = 1, \dots, N. \tag{5.7}$$

5.4. Lagrangian-random sampling (L-RS) scheme. We now summarize the Lagrangian-Random Sampling (L-RS) scheme for (1.1). Assume we have a numerical solution $\{\boldsymbol{\rho}_j^n\}_{j\in\mathbb{Z}}$ for time $t = t^n$ and wish to advance the solution to $t = t^{n+1} = t^n + \Delta t$, where Δt is subject to the CFL-type restriction (5.7). To this end the following two steps are performed successively:

1. *Lagrangian step.* Suppose that $\{\boldsymbol{\rho}_j^n\}_{j\in\mathbb{Z}}$ is an initial solution for

$$\partial_t \rho_i + \rho_i \partial_x v_i(\boldsymbol{\rho}) = 0, \quad i = 1, \dots, N.$$

   Then we obtain a numerical solution $\{\boldsymbol{\rho}_j^{n+1,-}\}_{j\in\mathbb{Z}}$ by the Lagrangian scheme (3.3).
2. *Random sampling remap step.* For $N = 1$, we use the two-state-per-cell random sampling step (5.3) to advance the solution to t^{n+1}. For $N > 1$, we approximately solve equation (5.5) with initial data $\{\boldsymbol{\rho}_j^{n+1,-}\}_{j\in\mathbb{Z}}$ by reconstructing a solution via (5.4) using the HLL approximate Riemann solver. After that, we perform the three-state-per-cell random sampling step (5.6) to obtain a numerical solution $\{\boldsymbol{\rho}_j^{n+1}\}_{j\in\mathbb{Z}}$ for $t = t^{n+1}$.

6. Numerical results.

6.1. CFL condition, errors, and entropy test. For $N = 1$ and a given value of Δx, we choose Δt so that $\lambda v_N^{\max} \le C_{\rm CFL}$ is satisfied with $C_{\rm CFL} = 0.95$ for the LR schemes and $C_{\rm CFL} = 0.8$ for Schemes 4 and 10, in agreement with the CFL condition stated in [8]. For $N > 1$, we use $C_{\rm CFL} = 0.9$ for all schemes. To evaluate the efficiency of the new schemes, for the examples addressing the case $N > 1$ plots of total (approximate) L^1 error versus CPU time are included. For $N = 1$, numerical solutions at moderately fine discretizations are compared with the exact entropy solution, while for $N > 1$, where no exact solution is at hand, we employ a reference solution obtained by a high-resolution spectral WENO scheme (WENO-SPEC; see [16]) with $\Delta x = 1/M_{\rm ref} = 1/25600$.

For $N > 1$ we only include numerical tests that turned out non-oscillatory results. In fact, multi-class versions of the L-UBee and L-rUBee schemes produced bounded but strongly oscillatory numerical results. For this reason, only the L-NBee version of L-AR schemes has been selected for further study and numerical tests for $N > 1$.

For the total L^1 error, we denote by $\{\rho_{i,j}^M(t)\}_{j=1}^{\mathcal{M}}$ and $\{\rho_{i,l}^{\rm ref}(t)\}_{l=1}^{\mathcal{M}_{\rm ref}}$ the numerical and reference solution for the i-th component at time t calculated with $\Delta x = 1/M$

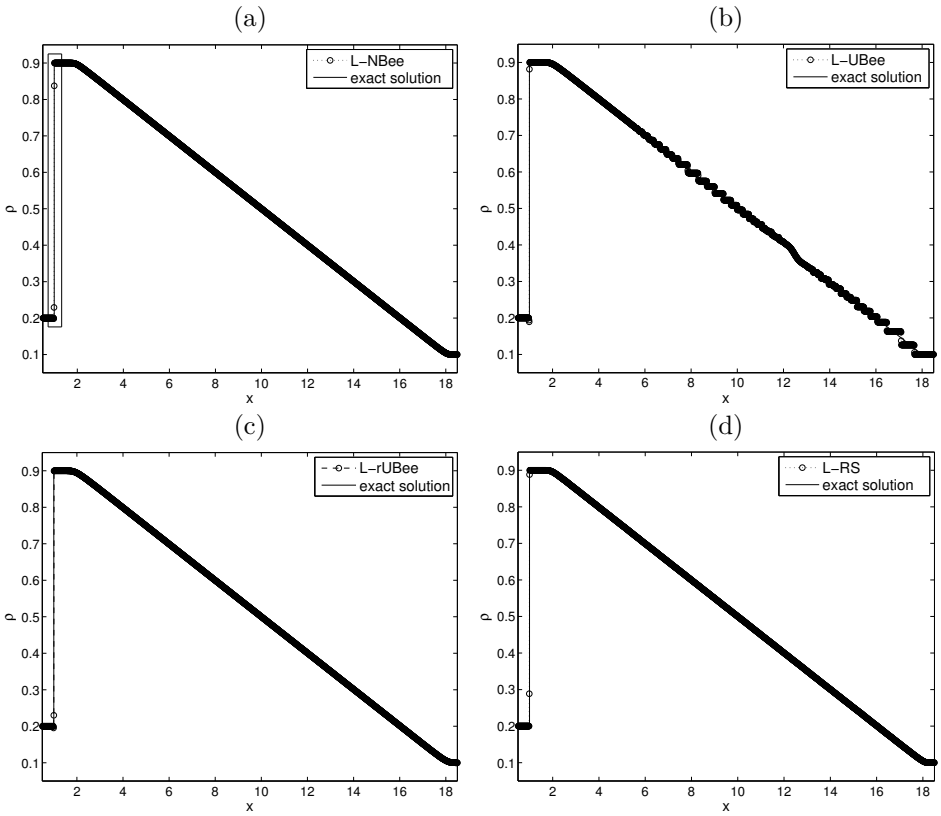

FIG. 6.1. *Example 1: numerical solution at* $t = 10$ *for* $\Delta x = 0.01$ *and schemes (a) L-NBee, (b) L-UBee, (c) L-rUBee, (d) L-RS.*

and $\Delta x = 1/M_{\text{ref}}$ using $\mathcal{M} = ML$ and $\mathcal{M}_{\text{ref}} = M_{\text{ref}}L$ cells, respectively. We use cubic interpolation from the reference grid to the $\mathcal{M}$ cells grid to compute $\widetilde{\rho}^{\text{ref}}_{i,j}(t)$ for $j = 1, \ldots, \mathcal{M}$. We then calculate the approximate L^1 error in species i by

$$e_i(t) := \frac{1}{M} \sum_{j=1}^{\mathcal{M}} \left| \widetilde{\rho}^{\text{ref}}_{i,j}(t) - \rho^M_{i,j}(t) \right|, \quad i = 1, \ldots, N.$$

The L-RS scheme described in Section 5 it is clearly non-conservative, since the remap step is based on random sampling. To measure the relative mass error as a function of time and Δx for the numerical solution for each species i, we evaluate

$$E_i(\Delta x; t) := \left| 1 - \frac{\Delta x}{m_i} \sum_{j=1}^{\mathcal{M}} \rho^n_{i,j} \right|, \quad m_i = \int_0^L \rho_{i,0}(x)\, \mathrm{d}x,$$

where $n = \lfloor t/\Delta t \rfloor$, m_i is the total "mass" of vehicles of class i, and $E_i(\Delta x; t)$ is the relative conservation of mass error of species i at time t in the interval $[0, L]$. In this way we define the total relative mass error by $E(\Delta x; t) = E_1(\Delta x; t) + \cdots + E_N(\Delta x; t)$, which overestimates the relative mass error in $\rho = \rho_1 + \cdots + \rho_N$.

Finally, in some cases we wish to test numerically whether the scheme under

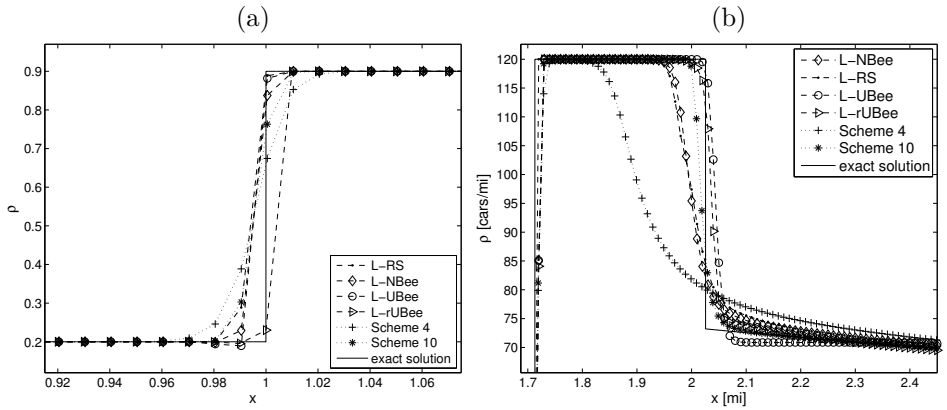

FIG. 6.2. *Enlarged views of (a) Example 1 at $t = 10$ (cf. Figure 6.1), (b) Example 2 at $t = 12.7$ (cf. Figure 6.5), calculated with $\Delta x = 0.01$ and including solutions by Schemes 4 and 10.*

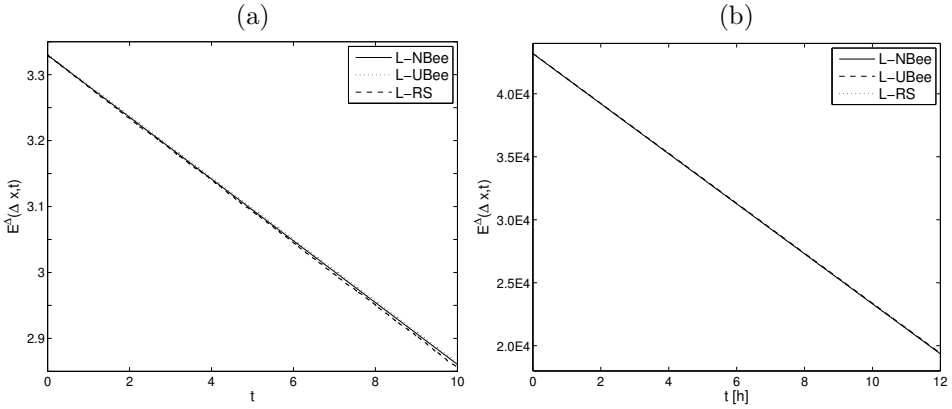

FIG. 6.3. *Entropy test for $\Delta x = 1/200$: (a) Example 1, (b) Example 2.*

consideration possibly approximates an entropy solution. To this end, we define

$$E^{\Delta}(\Delta x, t) := \Delta x \sum_{j=1}^{\mathcal{M}} U\big(\boldsymbol{\rho}_j^n\big), \quad \text{where } n = \lfloor t/\Delta t \rfloor. \tag{6.1}$$

Here $U(\boldsymbol{\rho})$ is a convex entropy function. For $N = 1$ we choose $U(\rho) = \rho^2/2$, and for $N > 1$ we choose $U(\boldsymbol{\rho}) = \mathcal{E}(\boldsymbol{\rho})$, where $\mathcal{E}(\boldsymbol{\rho})$ is defined in (2.6). In this form, and considering that in our examples the numerical solutions are compactly supported, for a given value of Δx the function $t \mapsto E^{\Delta}(\Delta x, t)$ must be non-increasing.

6.2. Example 1: $N = 1$, linear velocity. We consider (1.5) with $v(\rho)$ given by (1.6) with $v^{\max} = 1$ and $V(\rho)$ defined by (2.7) with $\rho_{\max} = 1$, along with

$$\rho(x, 0) = \rho_0(x) := \begin{cases} 0.2 & \text{for } x < 2, \\ 0.9 & \text{for } 2 \le x \le 9, \\ 0.1 & \text{for } x > 9. \end{cases}$$

TABLE 6.1
Example 1: L^1-errors (ERR; to be multiplied by 10^{-5}) and experimental orders of convergence (EOC) at $t = 10$ for three LR schemes and Schemes 4 and 10.

	L-rUBee		L-UBee		L-NBee		L-RS		Scheme 4		Scheme 10	
M	ERR	EOC	ERR	EOC	ERR	EOC	ERR	EOC	ERR	EOC	ERR	EOC
100	130.5	—	197.9	—	44.6	—	57.6	—	168.1	—	70.0	—
200	71.7	0.86	186.5	0.08	24.2	0.88	35.5	0.61	91.2	0.88	35.0	1.00
400	37.3	0.94	179.2	0.05	12.9	0.90	18.2	0.96	49.2	0.89	17.5	0.99
800	20.4	0.86	163.7	0.13	7.0	0.88	9.9	0.87	26.4	0.89	8.7	0.99
1600	10.7	0.92	159.2	0.04	3.6	0.92	5.4	0.86	14.1	0.90	4.3	1.00
3200	5.6	0.93	146.4	0.12	1.9	0.89	3.2	0.85	7.5	0.90	2.2	0.99
6400	2.9	0.94	134.8	0.11	1.0	0.90	1.5	1.08	3.9	0.91	1.1	1.00

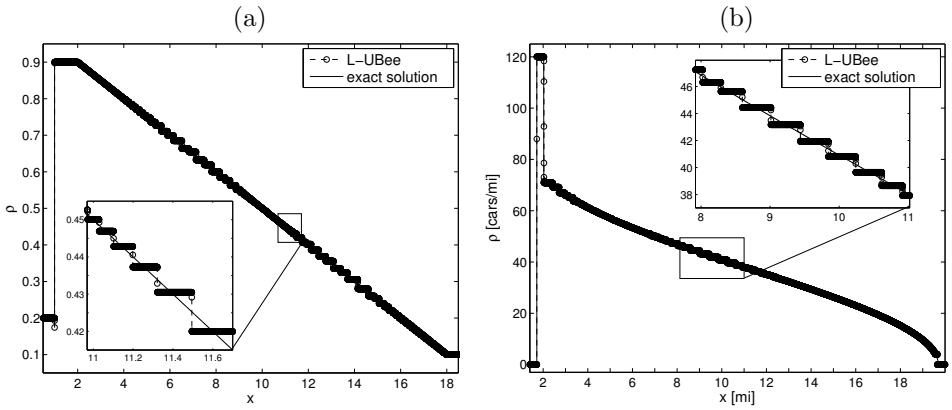

FIG. 6.4. *Numerical solution by scheme L-UBee, $\Delta x = 1/12800$: (a) Example 1, (b) Example 2.*

For this test, the flux $f(\rho) = \rho v(\rho)$ is concave ($f'' \equiv -2 < 0$), so according to the Lax entropy condition, the discontinuity in ρ_0 at $x = 2$ evolves as a shock propagating at speed $(f(0.9) - f(0.2))/(0.9 - 0.2) = -0.1$, while the jump in ρ_0 at $x = 9$ gives rise to a rarefaction wave centered at that position. Figure 6.1 shows numerical results at time $t = 10$, at which the shock of the exact solution and the rarefaction wave do not yet interact, i.e., on a short interval the solution value $\rho = 0.9$ is still present. The shock and the rarefaction wave are adequately approximated by the L-RS, L-rUBee and L-NBee schemes, while Figure 6.1 (b) indicates that the L-UBee scheme generates "stairs" in the rarefaction wave. An enlarged view around $x = 1$ is shown in Figure 6.2 (a), where numerical solutions are compared with those produced by Schemes 4 and 10. It appears that results by LR schemes are less diffusive those produced by other schemes.

Table 6.1 shows the error history, namely the approximate total L^1 error, experimental order of convergence EOC for Example 1 for different schemes. Clearly, for the L-NBee and L-RS schemes, the error goes to zero when the mesh is refined. In this example the values of the experimental orders of convergence EOC for LR schemes lie between those of Schemes 4 and 10.

As a consequence of Lemma 4.2, each scheme converges to a weak solution of (1.5). To determine whether this weak solution is an entropy solution, in Figure 6.3 (a), we plot the total entropy (6.1) as a function of t for each LR scheme, using $\Delta x = 1/200$.

TABLE 6.2
Relative mass errors $E(\Delta x; t)$ in dependence of $\Delta x = 1/M$ for the L-RS scheme.

	Example 1	Example 2	Example 4		Example 5	
M	$t = 10$	$t = 12.7$	$t = 0.03$	$t = 0.11$	$t = 0.03$	$t = 0.14$
100	3.45E-4	9.27E-3	2.82E-3	3.16E-3	6.65E-3	7.83E-3
200	8.72E-5	3.46E-3	2.34E-3	2.61E-3	2.32E-3	2.82E-3
400	8.60E-5	1.89E-3	1.81E-3	2.19E-3	6.07E-4	7.26E-4
800	3.37E-5	1.63E-3	7.60E-4	9.00E-4	3.48E-4	3.87E-4
1600	6.41E-6	1.59E-3	6.70E-4	8.50E-4	8.73E-5	1.04E-4
3200	4.22E-6	1.47E-3	5.40E-4	6.30E-4	2.11E-5	8.82E-5

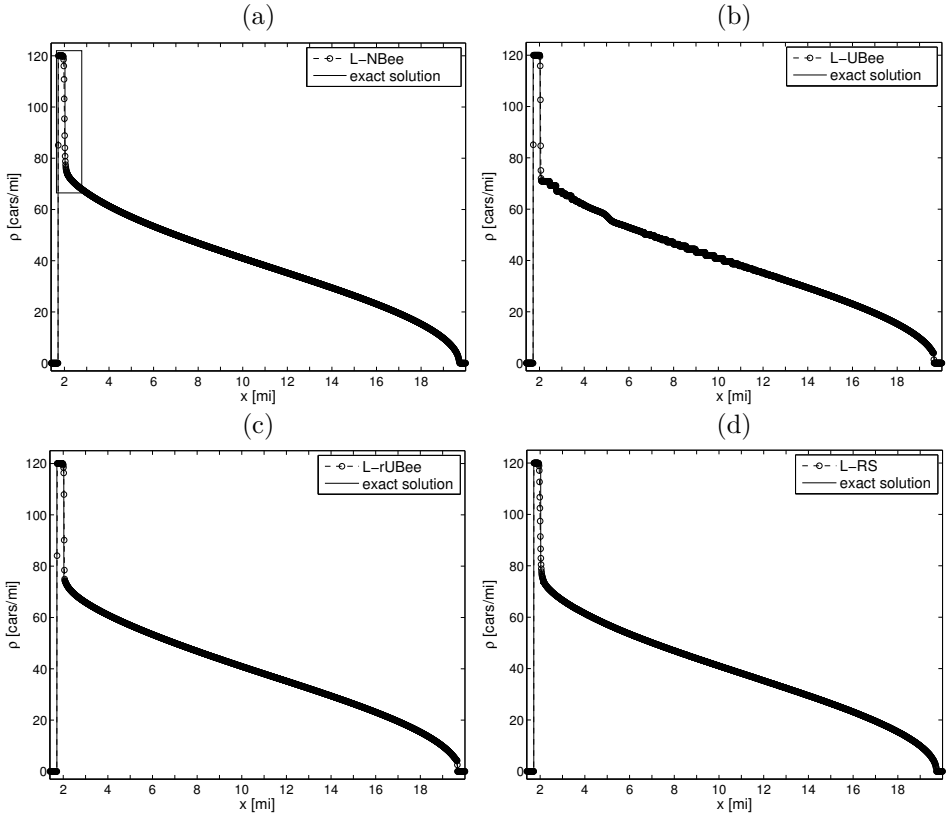

FIG. 6.5. *Example 2: schemes (a) L-NBee, (b) L-UBee, (c) L-rUBee, (d) L-RS at $t = 12.7$ with $\Delta x = 0.01$.*

We observe that $E^{\Delta}(\Delta x, t)$ is non-increasing in t. This behaviour is maintained when $\Delta x \downarrow 0$. Moreover, for the statistically conservative L-RS scheme,Table 6.2 shows the relative mass error at time $t = 10$ for different levels of discretization. For Example 1 the conservation error is small already for a coarse grid and decreases when $\Delta x \downarrow 0$.

In Figure 6.4 (a) we observe that when the mesh is refined, the numerical solution obtained with the L-UBee scheme produces "staircaising" that does not disappear upon refinement and the L^1-error is not appreciably reduced when $\Delta x \downarrow 0$. This phenomenon is due to the particular choice of the anti-diffusive scheme (UBee scheme) and has also been reported elsewhere for the linear advection, transport, and other equations [15] (see also [4, 5, 23, 24] and the references therein).

TABLE 6.3
Example 2: approximate L^1-errors (ERR, to be multiplied by 10^{-5}) and EOC for three LR schemes and Schemes 4 and 10 of [8] at simulated time $t = 12.7$.

	L-rUBee		L-UBee		L-NBee		L-RS		Scheme 4		Scheme 10	
M	ERR	EOC	ERR	EOC	ERR	EOC	ERR	EOC	ERR	EOC	ERR	EOC
100	110.9	—	202.7	—	141.9	—	191.0	—	440.0	—	72.2	—
200	67.2	0.72	170.1	0.25	78.5	0.85	98.2	0.94	258.0	0.76	35.6	1.02
400	40.0	0.74	143.6	0.24	39.9	0.97	51.2	0.95	147.6	0.80	15.2	1.22
800	25.2	0.66	133.3	0.10	23.4	0.76	33.0	0.63	85.9	0.78	8.4	0.84
1600	15.2	0.72	126.7	0.07	13.1	0.83	15.4	1.10	49.7	0.79	4.5	0.91
3200	8.5	0.83	122.1	0.05	7.1	0.88	9.1	0.75	28.1	0.81	2.2	1.03
6400	4.9	0.80	119.6	0.02	3.9	0.84	4.9	0.87	16.0	0.80	1.1	1.00

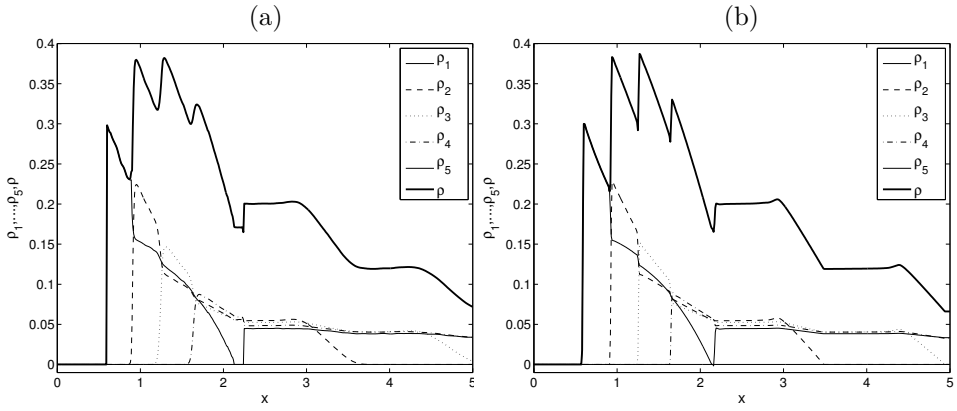

FIG. 6.6. *Example 3: numerical solution at $t = 7$ for $\Delta x = 0.01$ and schemes (a) L-RS, (b) L-NBee.*

6.3. Example 2: $N = 1$ exponential velocity. In this numerical test, we use a velocity function $v(\rho)$ given by (1.6) with $v^{\max} = 1$ and the hindrance function

$$V(\rho) = \exp\bigl(-(\rho/\rho^*)^2/2\bigr), \quad \rho^* = 50\,[\text{cars/mi}], \tag{6.2}$$

which was proposed by Drake [18], and an initial condition $\rho(x,0) = \rho_0(x)$ with $\rho(x) = 120\,\text{cars/mi}$ for $1 \le x \le 7$ and $\rho(x) = 0$ otherwise, where we employ the boundary conditions $\rho(0,t) = \rho(20,t) = 0$ for $t > 0$. For this test, the flux $f(\rho) = \rho v(\rho)$ is not concave, so the here entropy solution contains a shock and a rarefaction wave followed by a shock. Results at $t = 12.7$ are displayed in Figure 6.5. Figures 6.5 (a) and (b) show that the L-NBee and L-RS schemes adequately approximate the shock and the rarefaction wave, while Figure 6.5 (c) indicates that the L-UBee scheme produces staircasing in the rarefaction wave (as in the linear velocity case). The "stairs" do not disappear under refinement, as is shown in Figure 6.4 (b). For the L-RS scheme we observe in Table 6.2 that the relative mass error is small already for a coarse grid and decreases for $\Delta x \downarrow 0$. Table 6.3 shows L^1 errors and experimental orders of convergence EOC for Example 2 for different schemes. According to Table 6.3, the L-rUBee, L-NBee and L-RS schemes produce errors that lie between those of Schemes 4 and 10. In Figure 6.3 (b) we display the total entropy as a function of t. We observe that the function (6.1) is non-increasing in time.

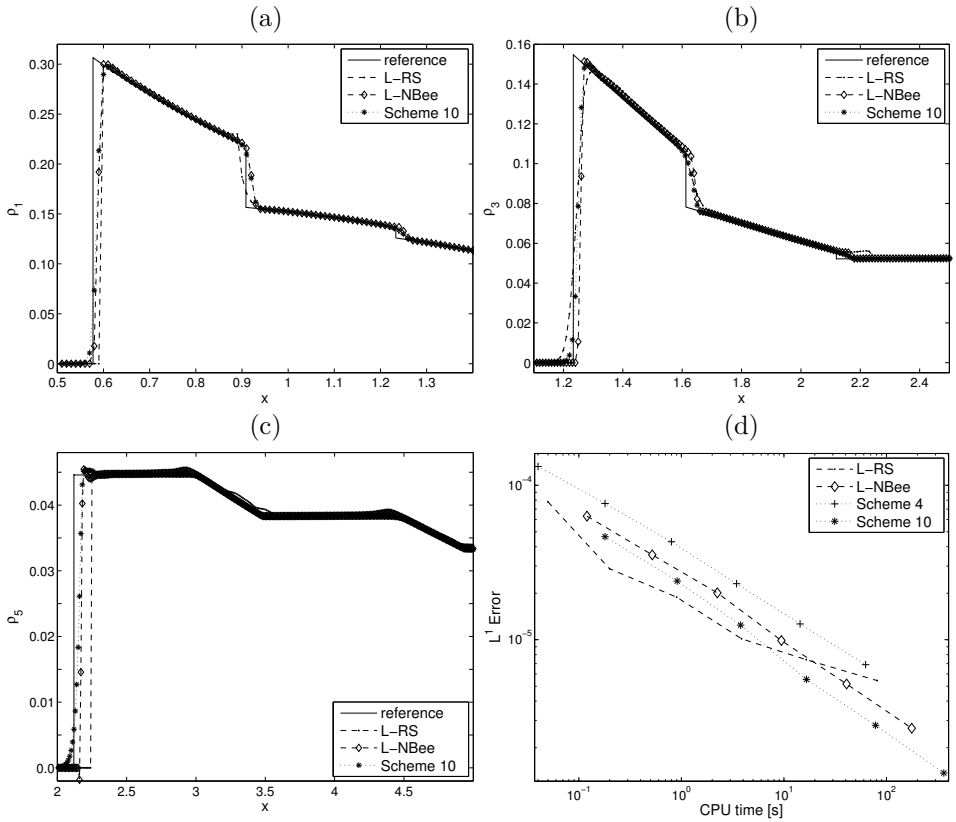

FIG. 6.7. *Example 3: (a–c) enlarged views of parts of Figure 6.6 for selected species, including numerical solutions by Schemes 4 and 10; (d) approximate total L^1 errors versus CPU time.*

TABLE 6.4
*Example 3: total approximate L^1 errors $e_{\rm tot}(t)$ (*ERR*, to be multiplied by 10^{-6}), EOC, and CPU times (*CPU*, in seconds) for two LR schemes and Schemes 4 and 10 at simulated time $t = 7$.*

	L-NBee			L-RS			Scheme 4			Scheme 10		
M	ERR	EOC	CPU	ERR	EOC	CPU	ERR	EOC	CPU	ERR	EOC	CPU
100	63.1	—	0.1	78.1	—	0.05	132.2	—	0.04	46.4	—	0.18
200	35.4	0.83	0.5	28.7	1.44	0.20	76.2	0.79	0.18	23.9	0.95	0.91
400	20.1	0.81	2.2	18.8	0.61	0.90	43.0	0.82	0.80	12.4	0.94	3.78
800	9.8	1.02	9.4	10.1	0.89	3.86	23.0	0.90	3.45	5.5	1.16	16.6
1600	5.1	0.93	40.8	7.4	0.55	16.49	12.6	0.86	14.38	2.7	0.98	78.3
3200	2.6	0.95	176.2	5.4	0.44	81.07	6.8	0.87	62.54	1.3	1.02	362.1

6.4. Example 3: $N = 5$, linear velocity. We consider the model (1.1) along with the hindrance function (2.7), $v_i^{\max} = i/N$, and the initial datum $\boldsymbol{\rho}(x,0) = \boldsymbol{\rho}_0(x)$ with $\boldsymbol{\rho}_0(x) = (0.2,\ldots,0.2)^{\rm T}$ for $0 \le x \le 1$ and $\boldsymbol{\rho}_0(x) = \mathbf{0}$ for $x < 0$ and $x > 1$.

In Figures 6.6 (a) and (b) we display the numerical solution obtained with the L-RS and L-NBee schemes, respectively, at simulated time $t = 7$ with $\Delta x = 1/100$. The solution produced by the L-NBee scheme appears to be less affected by numerical diffusion than the one corresponding to the L-RS scheme. In Figures 6.7 (a–c) enlarged views of the relevant parts for individual species are shown. Observe that the L-NBee

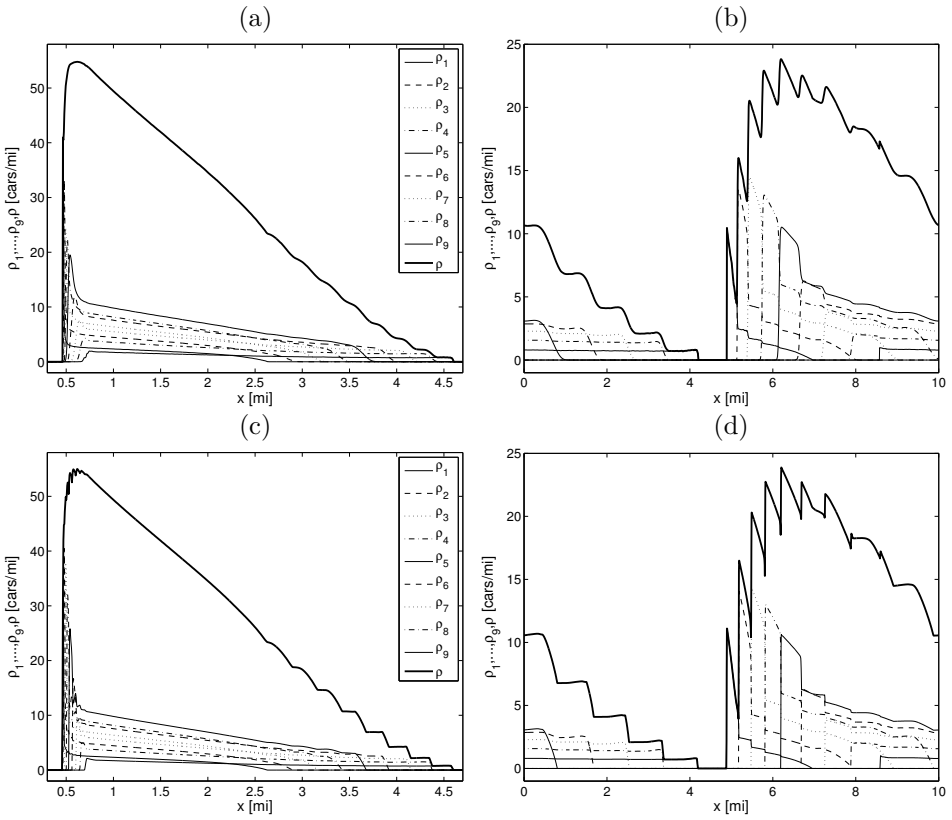

FIG. 6.8. *Example 4: schemes (a, b) L-RS, (c, d) L-NBee at (a, c)* $t = 0.03\,\mathrm{h}$*, (b, d)* $t = 0.11\,\mathrm{h}$*, and* $\Delta x = 1/200$*.*

scheme produces fairly sharp solutions in each individual species. Furthermore, note carefully that the numerical results of Figure 6.6 show that jumps in the total density ρ only occur from smaller to higher values in increaseing x-direction, in agreement with the entropy jump condition $\rho_- \leq \rho_+$ (cf. Section 2.1) valid for the present case.

6.5. Examples 4 and 5: $N = 9$, exponential velocity. We consider the MCLWR model (1.1) along with the hindrance function (6.2) and the numerical test proposed in [34], where $\boldsymbol{\rho}(x,0) = \boldsymbol{\rho}_0(x)$ describes an isolated platoon for (6.2) and $v_i^{\max} = (52.5 + 7.5i)\,\mathrm{mi/h}$, $i = 1,\ldots,9$. We consider a circular road of length $L = 10\,\mathrm{mi}$, i.e. we set $I := [0,10]$ with periodic boundary conditions, and set $\boldsymbol{\rho}_0(x) = 0.04p(x)\rho_0(1,2,3,4,5,4,3,2,1)^{\mathrm{T}}$, where

$$p\,(x) = \begin{cases} 10x & \text{for } 0 < x \leq 0.1, \quad 1 \quad \text{for } 0.1 < x \leq 0.9, \\ -10(x-1) & \text{for } 0.9 < x \leq 1, \quad 0 \quad \text{otherwise.} \end{cases}$$

In Example 4 we set $\rho_0 = 120\,\mathrm{cars/mi} > \rho^*$, which leads to a congested regime. In Example 5 we set $\rho_0 = 40\,\mathrm{cars/mi} < \rho^*$, which leads to a non-congested regime.

For Example 4, in Figures 6.8 (a) and (b) we display the numerical solution obtained with the L-RS scheme and in Figures 6.8 (c) and (d) those obtained with the L-NBee scheme at simulated times $t = 0.03\,\mathrm{h}$ and $t = 0.11\,\mathrm{h}$ with $\Delta x = 1/200\,\mathrm{mi}$.

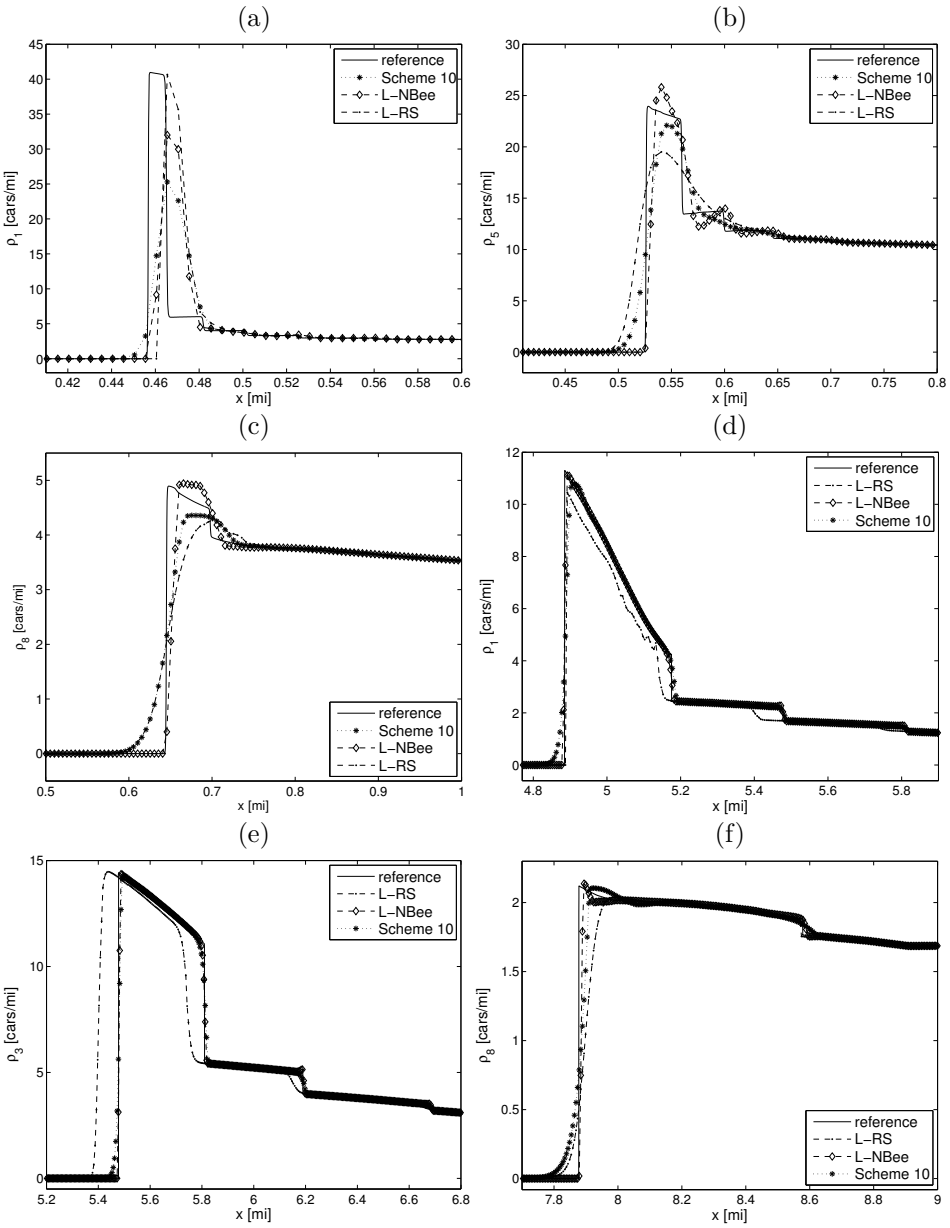

FIG. 6.9. *Example 4: enlarged views of parts of the numerical solutions of Figure 6.8 for selected species and (a–c)* $t = 0.03\,\mathrm{h}$*, (d–f)* $t = 0.13\,\mathrm{h}$*, including numerical solutions by Scheme 10.*

The traffic phenomenon is represented adequately by each scheme. Observe that the L-NBee scheme is more anti-diffusive than the L-RS scheme in this case. This behaviour is maintained for long simulated times. Enlarged views of relevant parts of the numerical solutions of Figure 6.8 for some selected species are shown in Figure 6.9. We compare the numerical solution for each species with a reference solution.

The numerical tests indicate that for several species, the numerical solution obtained by the L-NBee scheme are anti-diffusive in each species and this behaviour is

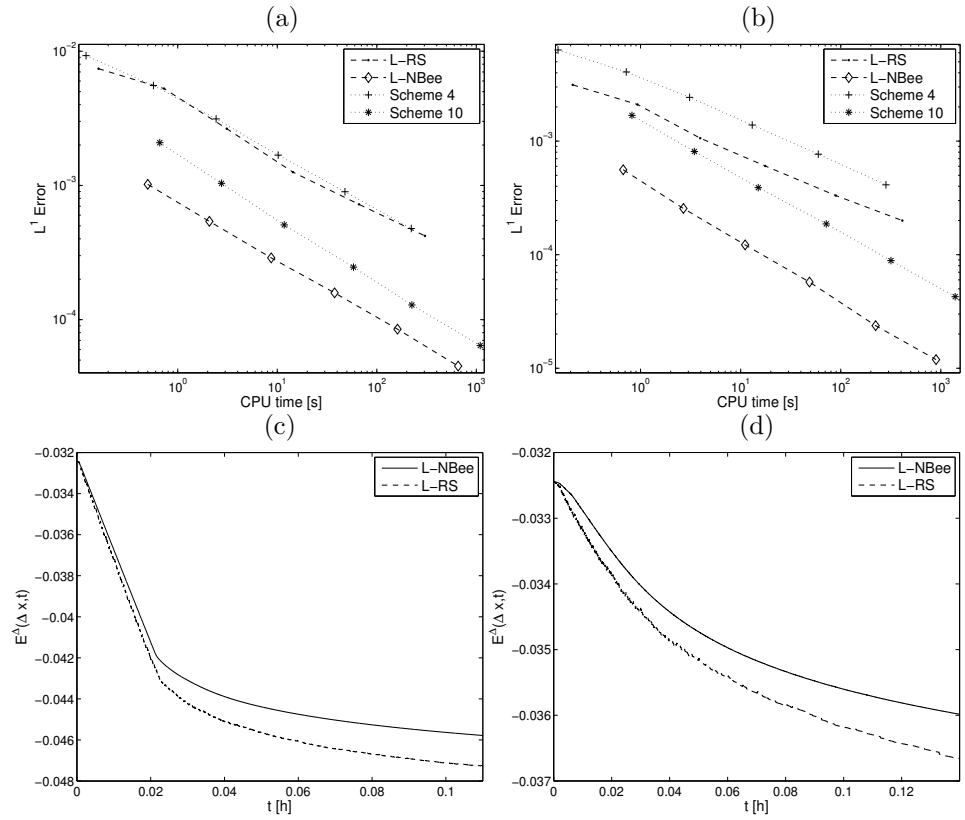

FIG. 6.10. *Approximate total L^1 error versus CPU time for (a) Example 4 at $t = 0.11\,\mathrm{h}$, (b) Example 5 at $t = 0.14\,\mathrm{h}$, and entropy test with $\Delta x = 1/200$ for (c) Example 4, (d) Example 5.*

maintained during a large portion of the simulated time, see Figure 6.9 for Example 4 and Figure 6.12 for Example 5. However, the L-RS scheme is more diffusive than Scheme 10, and in Figure 6.9 (e) we observe a delay in the approximation of the shock wave. This behaviour is observed for several individual species. As in the other examples, in Table 6.2 we observe that the relative mass error at a given simulated time decreases with the refinement of the mesh.

In Figures 6.10 (a) and (b) we display the efficiency of the numerical schemes in comparison with that of Schemes 4 and 10. We observe that the efficiency of the L-RS scheme is comparable with that of the first-order accurate Scheme 4, while the L-NBee scheme is even more efficient than the second-order accurate Scheme 10. In Figures 6.10 (c) and (d) we display the total entropy as a function of t, we observe that the function (6.1) is non-increasing in the time.

7. Conclusions. We have investigated a new class of numerical schemes for the challenging issue of approximating the solutions of the strongly coupled MCLWR models. These schemes are based on a Lagrangian-remap decomposition for each car density, and the use of anti-diffusive techniques for solving the remap step. The proposed strategies turn out to be very easy and competitive with respect to existent schemes, especially for large values of N (the number of densities or equivalently the size of the system), where no characteristic decomposition of the eigenstructure are

TABLE 6.5
Example 4: total approximate L^1 errors $e_{\text{tot}}(t)$ (ERR, to be multiplied by 10^{-5}), EOC, and CPU times (in seconds) for two LR schemes and Schemes 4 and 10.

		L-NBee			L-RS			Scheme 4			Scheme 10		
t	M	ERR	EOC	CPU	ERR	EOC	CPU	ERR	EOC	CPU	ERR	EOC	CPU
	100	684.9	—	0.07	1183.0	—	0.02	1197.7	—	0.01	670.7	—	0.09
	200	414.3	0.72	0.26	620.1	0.93	0.08	938.4	0.55	0.06	449.5	0.60	0.36
0.03	400	192.1	1.10	1.08	430.6	0.52	0.39	708.2	0.70	0.30	224.2	1.00	1.58
	800	83.7	1.19	4.42	300.1	0.52	1.68	507.9	0.77	1.32	110.4	1.02	6.96
	1600	47.0	0.83	19.16	220.0	0.44	7.45	321.3	0.86	5.50	51.4	1.10	34.2
	3200	31.4	0.68	83.36	130.7	0.75	36.7	185.1	0.89	24.58	29.8	0.78	152.6
	100	101.9	—	0.5	740.6	—	0.1	926.3	—	0.1	208.2	—	0.6
	200	53.9	0.91	2.0	526.7	0.49	0.7	555.6	0.73	0.5	103.6	1.00	2.7
0.11	400	28.8	0.90	8.7	264.6	0.99	3.1	313.1	0.82	2.4	50.8	1.02	11.7
	800	15.8	0.86	37.6	125.5	1.07	14.3	168.2	0.89	10.2	24.6	1.04	58.3
	1600	8.5	0.89	161.5	72.3	0.79	66.2	89.7	0.90	47.8	12.8	0.93	225.0
	3200	4.5	0.91	656.4	42.1	0.78	304.6	47.7	0.91	222.0	6.4	1.00	1094.9

TABLE 6.6
Example 5: total approximate L^1 errors $e_{\text{tot}}(t)$ (ERR, to be multiplied by 10^{-5}), EOC, and CPU times (in seconds) for two LR schemes and Schemes 4 and 10.

		L-NBee			L-RS			Scheme 4			Scheme 10		
t	M	ERR	EOC	CPU	ERR	EOC	CPU	ERR	EOC	CPU	ERR	EOC	CPU
	100	178.9	—	0.1	567.2	—	0.02	1037.8	—	0.01	386.3	—	0.1
	200	89.4	0.99	0.3	329.6	0.78	0.08	714.3	0.53	0.06	194.8	0.98	0.4
0.03	400	46.0	0.96	1.1	190.6	0.79	0.40	440.3	0.69	0.36	96.5	1.01	1.5
	800	20.7	1.14	4.4	92.3	1.04	1.64	243.3	0.85	1.29	45.6	1.08	6.5
	1600	8.9	1.21	18.8	47.3	0.96	7.44	126.1	0.94	5.38	20.2	1.17	32.3
	3200	4.4	1.01	83.3	28.3	0.74	37.73	65.3	0.94	24.16	10.1	1.00	146.0
	100	56.0	—	0.7	313.0	—	0.21	635.8	—	0.15	168.64	—	0.8
	200	25.5	1.13	2.7	210.6	0.57	0.93	406.6	0.64	0.72	81.15	1.05	3.5
0.14	400	12.2	1.06	11.1	106.1	0.98	3.95	242.8	0.74	3.09	38.97	1.05	15.0
	800	5.7	1.08	48.7	60.4	0.81	17.62	138.7	0.80	13.06	18.67	1.06	71.7
	1600	2.4	1.27	223.0	33.2	0.51	89.23	76.7	0.85	59.65	8.87	1.07	317.5
	3200	1.2	0.99	895.0	20.0	0.73	412.55	41.2	0.89	282.74	4.27	1.05	1389.7

needed and are stable up to a CFL number of 1.0. In the case $N = 1$, the strategy is supported by a partial numerical analysis since an L^∞ bound and a TVD property are established. Proving the validity of an entropy inequality is still an open problem at this stage but numerical experiments show the convergence to entropy solution.

In this first investigation we focus on traffic flow models for which the velocities $v_i(\rho) = v_i^{\max} V(\rho)$ are non-negative and such that $v'(\rho) \leq 0$. An interesting extension of this work could be envisaged to the polydisperse sedimentation models with velocities of variable sign [7]. The extension to second- or higher-order accuracy is a much more involved issue to be considered in the near future (even if the LR schemes are shown to be already competitive with second-order scheme "Scheme 10").

Acknowledgements. CC acknowledges F. De Vuyst for interesting discussions they had in 2010 on MCLWR traffic models. RB and CC acknowledge support by CNRS-Conicyt project. RB is supported by Fondecyt project 1130154; BASAL project CMM, U. de Chile and Centro de Investigación en Ingeniería Matemática (CI^{2}MA), U. de Concepción; Conicyt project Anillo ACT1118 (ANANUM); and Red Doctoral REDOC.CTA, MINEDUC project UCO1202 at U. de Concepción. LMV is supported by MECESUP project UCO0713.

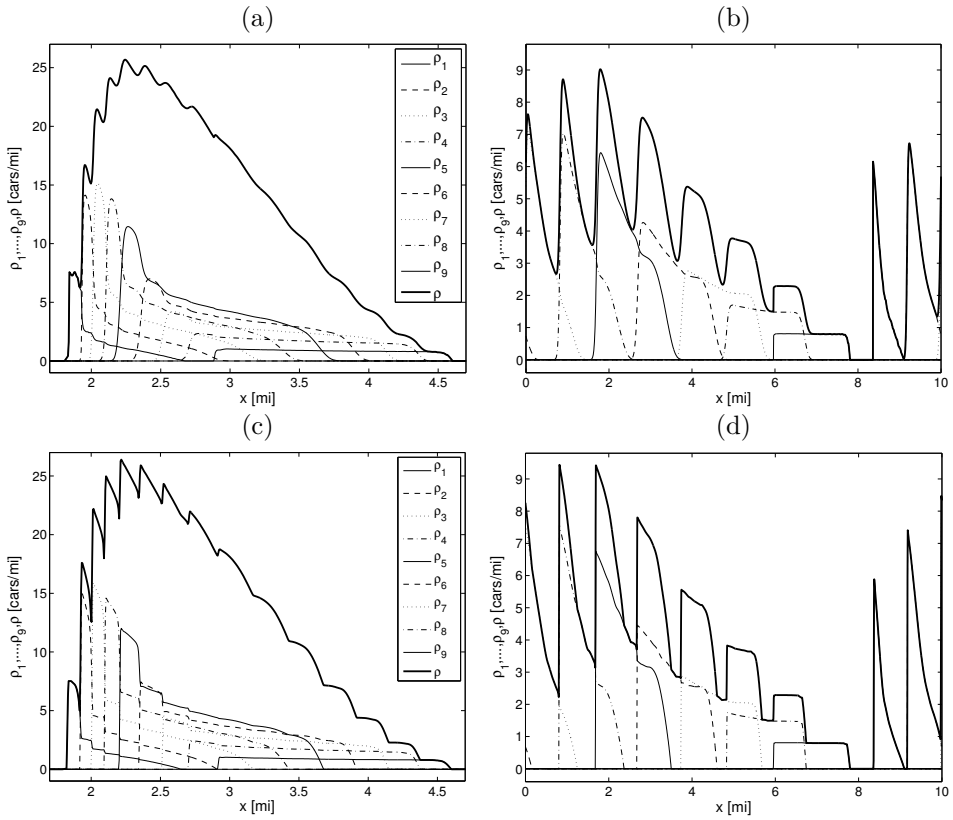

FIG. 6.11. *Example 5: schemes (a, b) L-RS, (c, d) L-NBee, (a, c)* $t = 0.03\,\mathrm{h}$*, (b, d)* $t = 0.14\,\mathrm{h}$*, and* $\Delta x = 1/200$*.*

REFERENCES

[1] M. BACHMANN, P. HELLUY, H. MATHIS, AND S. MÜLLER, *Random sampling remap for compressible two-phase flows.* Preprint (2010), see `http://hal.archives-ouvertes.fr/hal-00546919/fr/`

[2] S. BENZONI-GAVAGE AND R.M. COLOMBO, *An n-populations model for traffic flow*, Eur. J. Appl. Math., 14 (2003), pp. 587–612.

[3] S. BENZONI-GAVAGE, R.M. COLOMBO, AND P. GWIAZDA, *Measure valued solutions to conservation laws motivated by traffic modelling*, Proc. Royal Soc. A, 462 (2006), pp. 1791–1803.

[4] O. BOKANOWSKI AND H. ZIDANI, *Anti-dissipative schemes for advection and application to Hamilton-Jacobi-Bellman equations*, J. Sci. Comput., 30 (2007), pp. 1–33.

[5] F. BOUCHUT, *An anti-diffusive entropy scheme for monotone scalar conservation laws*, J. Sci. Comput., 21 (2004), pp.1–30.

[6] A. BRESSAN, *Hyperbolic Systems of Conservation Laws*, Oxford University Press, 2000.

[7] R. BÜRGER, R. DONAT, P. MULET, AND C.A. VEGA, *On the implementation of WENO schemes for a class of polydisperse sedimentation models*, J. Comput. Phys., 230 (2011), pp. 2322–2344.

[8] R. BÜRGER, A. GARCÍA, K.H. KARLSEN, AND J.D. TOWERS, *A family of numerical schemes for kinematic flows with discontinuous flux*, J. Eng. Math., 60 (2008), pp. 387–425.

[9] R. BÜRGER, K.H. KARLSEN, AND J.D. TOWERS, *On some difference schemes and entropy conditions for a class of multi-species kinematic flow models with discontinuous flux*, Netw. Heterog. Media, 5 (2010), pp. 461–485.

[10] R. BÜRGER, P. MULET, AND L.M. VILLADA, *Regularized nonlinear solvers for IMEX methods applied to diffusively corrected multi-species kinematic flow models*, SIAM J. Sci. Comput.,

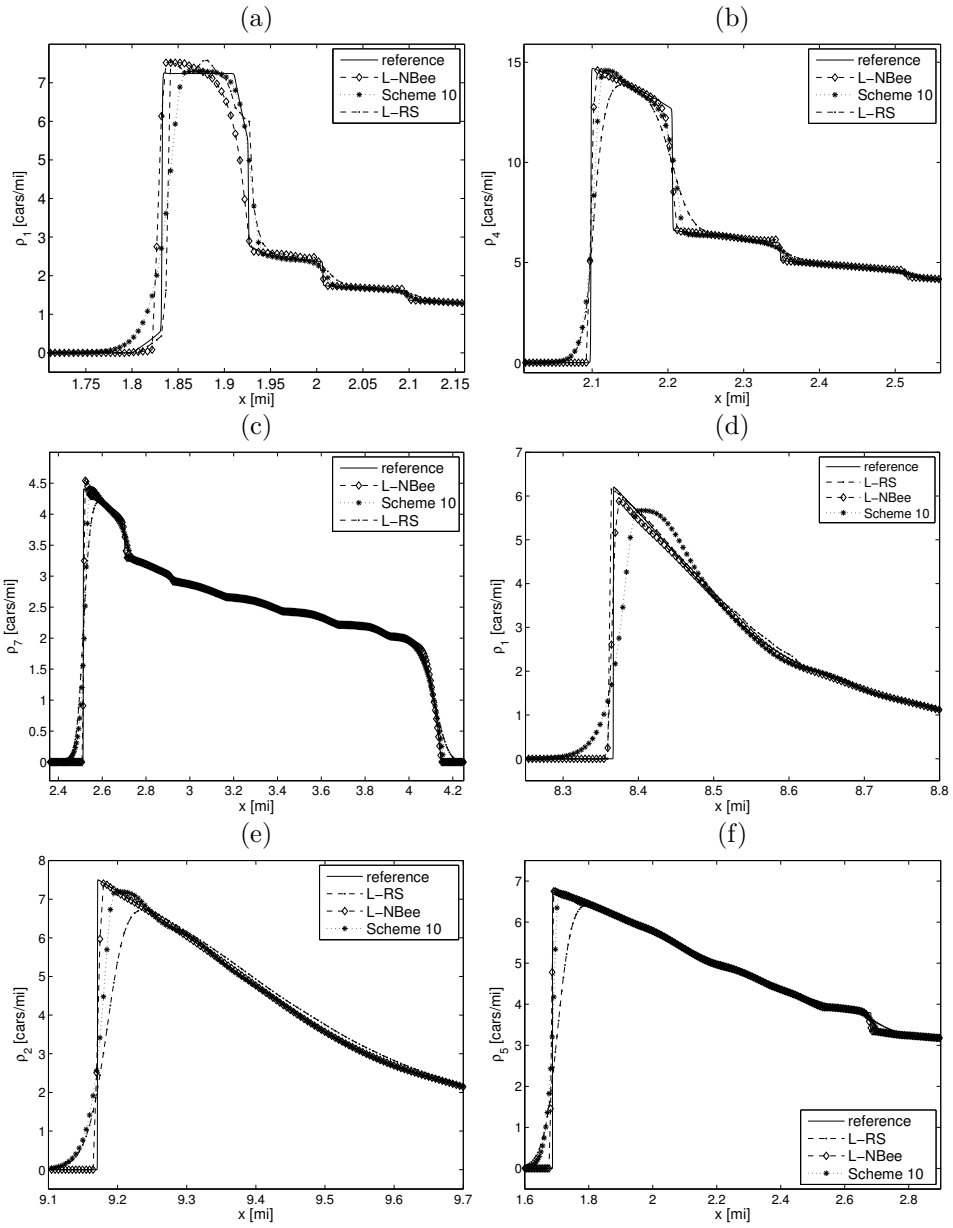

FIG. 6.12. *Example 5: enlarged views of parts of the numerical solutions of Figure 6.11 for selected species and (a–c)* $t = 0.03\,\mathrm{h}$*, (d–f)* $t = 0.14\,\mathrm{h}$*, including numerical solutions by Scheme 10.*

to appear.

[11] C. CHALONS, *Transport-equilibrium schemes for computing nonclassical shocks. Scalar conservation laws*, Numer. Meth. Partial Diff. Eqns., 24 (2008), pp. 1127–1147.

[12] C. CHALONS AND F. COQUEL, *Computing material fronts with a Lagrange-projection approach*, in: T. LI AND S. JIANG (eds.), *Hyperbolic Problems: Theory, Numerics and Applications*. Series in Contemporary Applied Mathematics CAM 17/18, vol. 1. Higher Education Press, Beijing, China, pp. 346–356, 2012.

[13] C. CHALONS AND P. GOATIN, *Transport-equilibrium schemes for computing contact disconti-*

nuities in traffic flow modeling, Commun. Math. Sci., 3 (2007), pp. 533–551.
[14] C. Chalons and P. Goatin, *Godunov scheme and sampling technique for computing phase transitions in traffic flow modeling*, Interfaces Free Boundaries, 10 (2008), pp. 197–221.
[15] B. Després and F. Lagoutière, *Contact discontinuity capturing schemes for linear advection and compressible gas dynamics*, J. Sci. Comput., 16 (2001), pp. 479–524.
[16] R. Donat and P. Mulet, *Characteristic-based schemes for multi-class Lighthill-Whitham-Richards traffic models*, J. Sci. Comput., 37 (2008), pp. 233–250.
[17] R. Donat and P. Mulet, *A secular equation for the Jacobian matrix of certain multi-species kinematic flow models*, Numer. Meth. Partial Diff. Eqns., 26 (2010), pp. 159–175.
[18] J.S. Drake, J.L. Schofer, and A.D. May, *A statistical analysis of speed density hypothesis*, Highway Res. Record, 154 (1967), pp. 53–87.
[19] J. Glimm, *Solutions in the large for nonlinear hyperbolic systems of equations*, Comm. Pure Appl. Math., 18 (1965), pp. 697–715.
[20] E. Godlewski and P.-A. Raviart, *Numerical Approximation of Hyperbolic Systems of Conservation Laws*, Springer Verlag, New York, 1996.
[21] P. Helluy and J. Jung, *A coupled well-balanced and random sampling scheme for computing bubble oscillations*, ESAIM Proc., 35 (2012), pp. 245–250.
[22] M. Herty, C. Kirchner, and S. Moutari, *Multi-class traffic models on road networks*, Commun. Math. Sci., 4 (2006), pp. 591–608.
[23] S. Jaouen and F. Lagoutière, *Numerical transport of an arbitrary number of components*, Comput. Meth. Appl. Mech. Engrg., 196 (2007), pp. 3127–3140.
[24] F. Lagoutière, *Stability of reconstruction schemes for hyperbolic PDEs*, Commun. Math. Sci., 6 (2008), pp. 57–70.
[25] A. Harten, P.D. Lax, and B. van Leer, *On upstream differencing and Godunov-type schemes for hyperbolic conservation laws*, SIAM Rev., 25 (1983), pp. 35–61.
[26] M.J. Lighthill and G.B. Whitham, *On kinematic waves: II. A theory of traffic flow on long crowded roads*, Proc. Royal Soc. A, 229 (1955), pp. 317–345.
[27] S. Logghe and L.H. Immers, *Multi-class kinematic wave theory of traffic flow*, Transp. Res. B, 42 (2008), pp. 523–541.
[28] D. Ngoduy, *Multiclass first-order modelling of traffic networks using discontinuous flow-density relationships*, Transportmetrica, 6 (2010), pp. 121–141.
[29] D. Ngoduy, *Multiclass first-order traffic model using stochastic fundamental diagrams*, Transportmetrica, 7 (2011), pp. 111–125.
[30] P.I. Richards, *Shock waves on the highway*, Oper. Res., 4 (1956), pp. 42–51.
[31] J. Smoller, *Shock Waves and Reaction-Diffusion Equations*, Springer-Verlag, New York, 1983.
[32] E.F. Toro, *Riemann Solvers and Numerical Methods for Fluid Dynamics*, Third Edition, Springer-Verlag, Berlin, 2009.
[33] B. van Leer, *Towards the ultimate conservative difference scheme II. Monotonicity and conservation combined in a second order scheme*, J. Comput. Phys., 14 (1974), pp. 361–370.
[34] G.C.K. Wong and S.C. Wong, *A multi-class traffic flow model—an extension of LWR model with heterogeneous drivers*, Transp. Res. A, 36 (2002), pp. 827–841.
[35] Z. Xu and C.-W. Shu, *Anti-diffusive flux corrections for high order finite difference WENO schemes*, J. Comput. Phys., 205 (2005), pp. 458–485.
[36] M. Zhang, C.-W. Shu, G.C.K. Wong, and S.C. Wong, *A weighted essentially non-oscillatory numerical scheme for a multi-class Lighthill-Whitham-Richards traffic flow model*, J. Comput. Phys., 191 (2003), pp. 639–659.
[37] P. Zhang, R.-X. Liu, S.C. Wong, and S.Q. Dai, Hyperbolicity and kinematic waves of a class of multi-population partial differential equations. *Eur. J. Appl. Math.*, 17:171–200, 2006.
[38] P. Zhang, S.C. Wong, and C.-W. Shu, *A weighted essentially non-oscillatory numerical scheme for a multi-class traffic flow model on an inhomogeneous highway*, J. Comput. Phys., 212 (2006), pp. 739–756.